ELASTIC AND INELASTIC

NEUTRON SCATTERING CROSS SECTIONS

FOR

^{10}B, ^{11}B AND ^{16}O

by

Sharon Gail Glendinning
Department of Physics
Duke University

Date:_____

Approved:

_____
Edward G. Bilpuch, supervisor

_____

_____

_____

Dissertation submitted in partial fulfillment of the requirements for the degree of Doctor of Philosophy in the Department of Physics in the Graduate School of Duke University

1980

Abstract

Physics - Nuclear

ELASTIC AND INELASTIC

NEUTRON SCATTERING CROSS SECTIONS

FOR

^{10}B, ^{11}B AND ^{16}O

by

Sharon Gail Glendinning
Department of Physics
Duke University

Date:_____

Approved:

_____
Edward G. Bilpuch, supervisor

_____

_____

_____

An abstract of a dissertation submitted in partial fulfillment of the requirements for the degree of Doctor of Philosophy in the Department of Physics Physics in the Graduate School of Duke University

1980

Abstract

Neutron scattering cross sections of high quality have been measured for ^{10}B, ^{11}B and ^{16}O using the Triangle Universities Nuclear Laboratory neutron time-of-flight facility. These data are useful both for the CTR program and for studies of the isospin dependence of the nuclear force. The neutron data obtained are compared with high quality proton data for ^{10}B to determine this dependence using the optical model, assuming that the isospin dependence may be expressed as a correction to the energy of the incident projectile. The energy correction is found to be 4.6 ± 1.4 MeV lowering of the incident energy for protons. The neutron data obtained for ^{11}B were compared to the ^{10}B neutron and proton data in an attempt to extract the symmetry terms (dependence on target isospin) but the data were insufficiently sensitive to this effect to yield good results. The spherical optical model alone was insufficient to predict the ^{16}O data because of the many resonances in the energy region, so a model which allowed the addition of resonances to an optical model background was used for these data. Three resonances were added to an optical model background and tentative spin-parity and width assignments were made which gave a noticable improvement in the fits to the data. The ^{11}B data (elastic and inelastic) were also fit using the coupled-channel optical model. A value for the coupling parameter was obtained from hyperfine structure results for the electric quadrupole moment in the

literature.

ACKNOWLEDGEMENTS

I would like to express my gratitude to all the members of the neutron time-of-flight group, particularly Dr. F.O.Purser for his guidance and assistance at all phases of this work, and Drs. C.R.Gould, C.E.Nelson and H.H.Hogue for many instances of helpful discussions. I would also like to thank TUNL director Dr. E.G.Bilpuch for giving me the opportunity to work with the time-of-flight program. I would like to thank A.G.Beyerle, S.El-kadi and Dr. L.W.Seagondollar for their assistance in obtaining the data in this work. All of these people took part in an extensive modification and improvement of the time-of-flight facility in the years 1977 - 1978.

I would like also to express my appreciation to Mrs. Dorothy (Mike) Bailey for drawing the figures in this work and to Carey Floyd for his work in photographing them; and, finally, to my parents for their support and patience throughout.

This work was supported by the United States Department of Energy.

S.G.G.

TABLE OF CONTENTS

LIST OF TABLES

LIST OF FIGURES

Chapter I

INTRODUCTION

During the years 1975 through 1978 neutron scattering data of high quality were measured at TUNL for the nuclei ^{10}B, ^{11}B and ^{16}O for incident neutron energies between 8 and 15 MeV. These data complete the study of neutron scattering from p - shell elements which was begun in 1974 and reported in the thesis of H.Hogue, among other publications [1 - 4]. A summary of the data measured thus far is shown in Table 1. The earlier data were analyzed using optical models, specifically the spherical optical model and the coupled - channel model of T.Tamura [5], [6]. The present work considers the data for the three nuclei ^{10}B, ^{11}B and ^{16}O using similar techniques. The results of this investigation confirm the earlier conclusion that these models provide a fair approximation to the data.

In recent years with the prospect of controlled thermonuclear reactors becoming a matter of intense interest, a need has grown for neutron cross section data in the energy region from thermal neutrons to 14 MeV, this being the region of neutrons produced from the $D(t,n)^4He$ reaction. While data has been measured for very low energy neutrons and for neutrons at 14 MeV for many elements, there has

TABLE 1

Summary of Neutron Scattering Data

Nucleus	Differential Cross section	Angles (lab) No.	Angles (lab) Range	Energies (lab) No.	Energies (lab) Range (MeV)
^{6}Li	Elastic	28	25° - 160°	7	7.5 - 14
^{6}Li	Inelastic Q = -2.18 MeV	28	25° - 160°	7	7.5 - 14
^{7}Li	Elastic	28	25° - 160°	8	7 - 14
^{7}Li	Inelastic Q = -4.68 MeV	28	25° - 160°	6	9 - 14
^{9}Be	Elastic	28	25° - 160°	8	7 - 14
^{9}Be	Inelastic Q = -2.18 MeV	28	25° - 160°	8	7 - 14
^{10}B	Elastic	27	25° - 155°	7	8 - 14
^{10}B	Inelastic Q = -.707 MeV	15 9	40° - 155° 100° - 155°	1 6	8 9 - 14
^{11}B	Elastic	27	25° - 155°	8	8 - 14
^{11}B	Inelastic Q = -2.14 MeV	27	25° - 155°	8	8 - 14
^{11}B	Inelastic Q = -4.46 MeV	27	25° - 155°	8	8 - 14
^{11}B	Inelastic Q = -5.04 MeV	27	25° - 155°	7	9 - 14
^{12}C	Elastic	28	25° - 160°	15	9 - 15
^{12}C	Inelastic Q = -4.44 MeV	28	25° - 160°	15	9 - 15
^{16}O	Elastic	28	25° - 160°	11	9.25 - 15

remained a gap in the data for neutrons between about 8 MeV and 14 MeV. The neutron time-of-flight facility at TUNL has been designed to measure neutron scattering cross sections in precisely this energy range.

Among the elements for which data are urgently needed for the fusion program are all of the p-shell elements, as most of these elements are present in reactor designs as neutron moderating materials. It is desired also to know neutron cross section data for these materials in order to form estimates of the damage caused to reactor structures by high neutron flux.

The validity of the optical model as a description of nucleon scattering has been known since 1954 [7]. That it is applicable for scattering from targets of low mass might be questionable since this would appear to violate one of the basic assumptions of the optical model, that the nuclear matter is a smooth isotropic distribution. However, previous work in this area by Hogue (1977) and Watson [8] has demonstrated that it is possible to find parameter sets which, while providing excellent fits to measured data, yet vary smoothly with energy and target mass. Thus, the applicability of the model to p-shell nuclei is borne out by its success. Neutron data are of great usefulness in carrying out an optical model study of a given nucleus, as, when compared to proton scattering data, a measure of the isospin

dependence of the nuclear force is obtained. Especially, if the target nucleus has zero isospin, a direct measure of the projectile isospin dependence is obtained. This is the case for the target nucleus ^{10}B, for which both high quality neutron and proton scattering data are available. A study is made here using the computer program GENOA [10] developed by F. Perey of ORNL. This program has the capability of finding a set of optical model parameters which best fits several sets of data simultaneously, and to search specifically for the best isospin dependence.

The addition of ^{11}B data to the available ^{10}B data should provide a measure of the dependence of the model on the target isospin. This dependence is normally expressed as a correction to the real and imaginary well depths; it was found however that the data were not sensitive enough to these corrections to provide a good estimate of this dependence.

While for ^{10}B and ^{11}B most of the data measured lie in an energy region above most single particle resonances, which are specifically excluded from consideration in most optical model treatments, for the ^{16}O data this was not the case. It should be impossible to adequately predict the oxygen scattering data with a simple optical model, and this indeed was the case. However, a computer program developed by W. Thompson of UNC allows the addition of single-particle reso-

nances to an optical model background rather than the usual hard-sphere background suitable to lower energies. This approach proved useful for dealing with the oxygen scattering data.

In the coupled-channel optical model of Tamura, a method is developed for predicting scattering which leaves the target nucleus in an excited state by assuming that this excited state is a collective excitation of the nucleus. Two forms of collective excitation are allowed in this model: vibrational excitation (useful when considering nuclei which have no permanent deformation) and rotational excitation (useful for nuclei which are permanently deformed). ^{11}B is a nucleus which is permanently deformed, and the ground state and the second excited state form the first two members of a possible rotational band. For this reason, it was decided to use this model (in the form of the computer code JUPITOR) to perform calculations for the ^{11}B data. The results obtained provide good estimates for the angular distributions but fail to exactly reproduce the detailed structure of the distributions.

Chapter II

EXPERIMENTAL DETAIL

The data for oxygen and most of the data for ^{11}B were taken using the time-of-flight facility described in detail elsewhere (Hogue, 1977). However, considerable modification was done to the system before the ^{10}B study was begun. The new setup will be described here.

2.1 NEUTRON SOURCE

Neutrons for all the data contained in this work were produced by bombarding a deuterium gas cell with a pulsed and bunched beam of accelerated deuterons. The deuterons originate in the ion source DENIS II (see Figure 1), are chopped and bunched at position 2, are accelerated by the tandem van de Graaff (3), and are deflected to the time-of-flight target area (4).

The new deuteron source is a direct extraction negative ion source capable of delivering an 85 μA DC beam of negatively charged deuterons. The beam is passed through an HVEC RF chopper which sweeps it across a 0.375 inch aperture at a frequency of 2 MHz. The retrace pulse is removed by an auxiliary chopping voltage which puts out a square wave at a rate of 2 MHz. The pulse so produced is narrowed without

Figure 1: Floor plan of the laboratory.

Cyclo-Graaff Laboratory

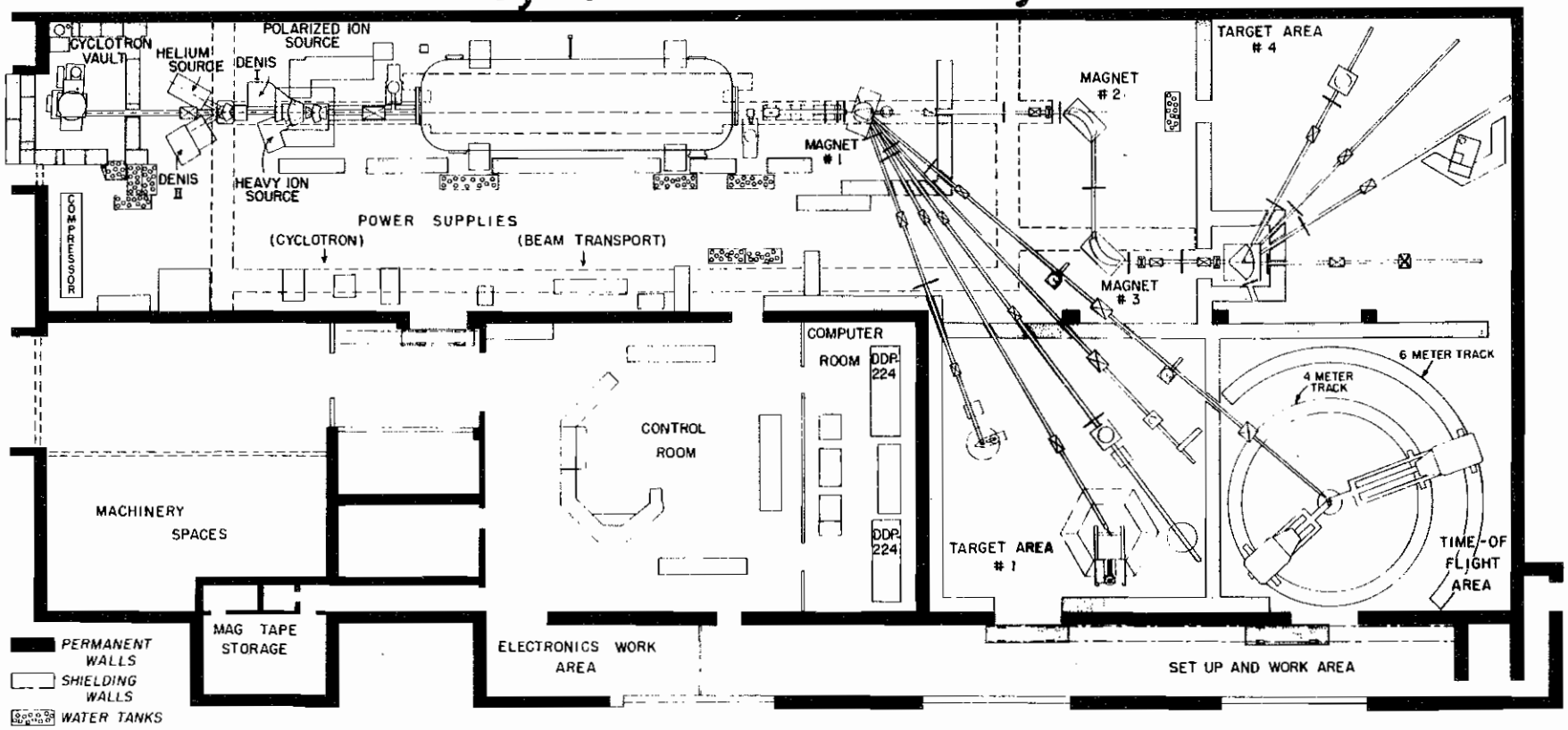

loss of beam by a two-gap klystron buncher; the final beam pulse has a nearly gaussian shape and a FWHM of about 2 ns.

The beam is accelerated by the tandem van de Graaff accelerator; typically, the voltage on the terminal was between 2.0 and 6.0 MV. Such voltages produced neutron beams with energies between 8.0 and 15.0 MeV. The positive beam so produced is deflected by the 20° - 70° bending magnet through an angle of 38° down the time-of-flight beam leg. One of the primary concerns in designing a beam leg for neutron work is the elimination of all sources of contamination by carbon - containing compounds. Contamination of this sort will produce groups of neutrons in the source spectrum which cannot be corrected for with sample out background runs. In order to avoid time-consuming gas out runs, efforts were made to reduce such contaminants to a minimum. Thus, the beam leg is carefully constructed with indium vacuum seals to eliminate the possibility of carbon contamination from conventional O-rings. The beam leg has three pumping stations and three quadrupole lenses (see Figure 1). It is pumped to a vacuum of about 2 * 10^{-6} torr with two conventional diffusion pumps and one titanium sublimation pump. Usually up to about 3 μA of beam could be delivered on target, for a transmission through the beam leg of 90%.

Contamination of the system by carbon compounds is further reduced by the use of cryogenic traps near the gas cell. The deuterium gas cell is shown in Figure 2.

Figure 2: Schematic diagram of the deuterium gas cell.

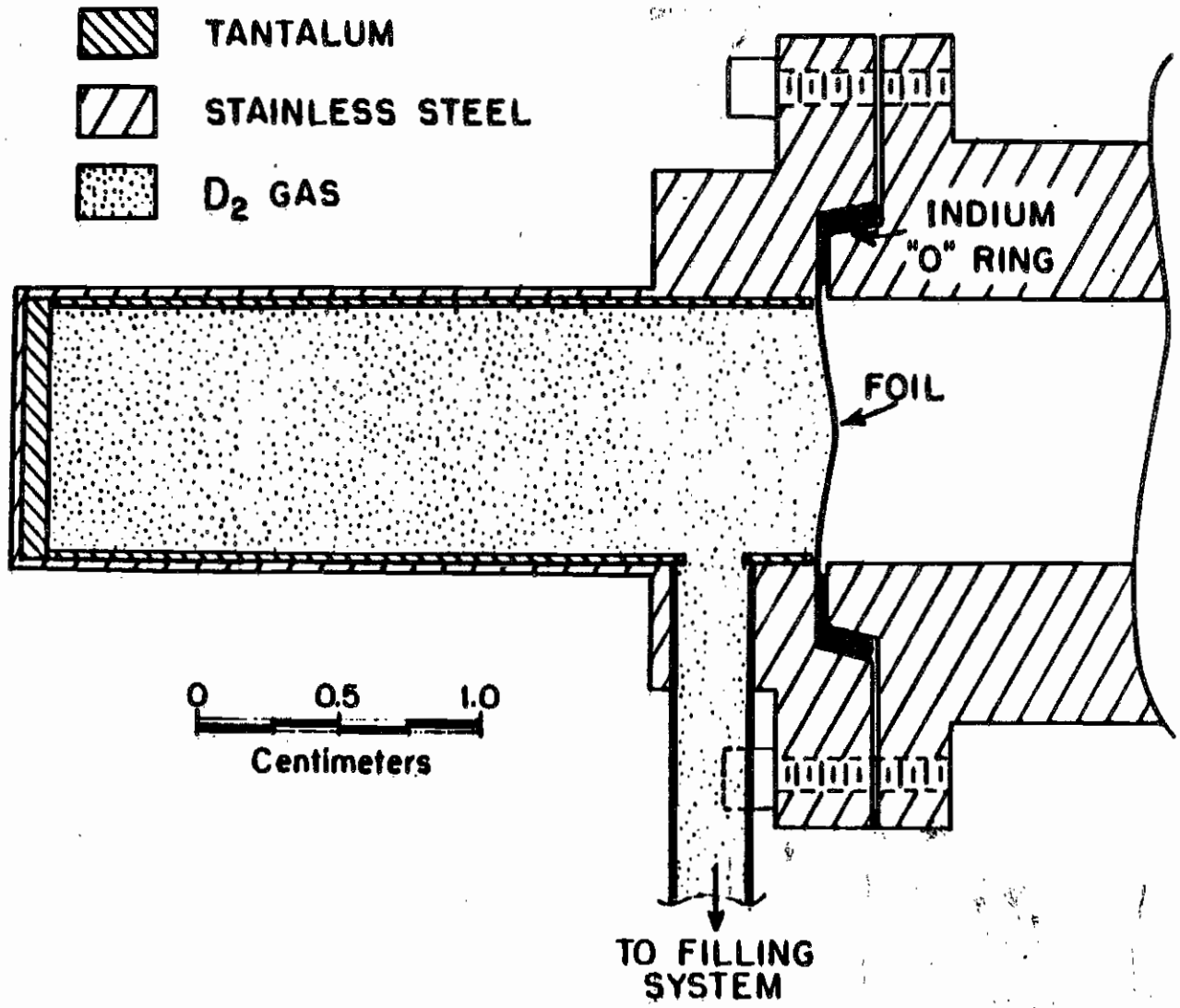
TANTALUM
STAINLESS STEEL
D_2 GAS
INDIUM "O" RING
FOIL
0
0.5
1.0
Centimeters
TO FILLING SYSTEM

The outer wall was made of stainless steel and was lined with a tantalum shell, used because of the low d,n cross section. The foil between beam leg vacuum and gas cell was made of 3.5 μm molybdenum. The foil was sealed to the gas cell and to the beam tube by an O - ring made of 0.030 inch indium wire. The gas cell, liners, O - ring and foil were thoroughly cleaned in a 1 molar solution of NaOH, and the liners were further cleaned in a 50% solution of HF. All were then rinsed several times in distilled water and carefully dried. This procedure is useful in removing any trace of carbon compounds found on the gas cell components.

The gas cell is filled to a pressure of about 30 psi absolute with 99.99% pure deuterium. The deuterium is passed through a liquid nitrogen cold trap to remove traces of water, grease, and any other impurities. The filling system is at a distance of about 18 inches above the beam line to reduce the extra mass near the gas cell, and the cell itself is filled via a stainless steel capillary tube.

2.2 TIME-OF-FLIGHT SPECTROMETER

A new detector assembly was recently added to the time-of-flight facility. The detector is a 5 inch diameter by 2 inch thick NE-218 liquid organic scintillator which is optically coupled to an XP - 2041 Amperex photomultiplier tube. Surrounding the detector is a massive (4700 kg.) shield and collimator. The schematic for this is shown in Figure 3.

Figure 3: Schematic diagram of the detector shield and collimator.

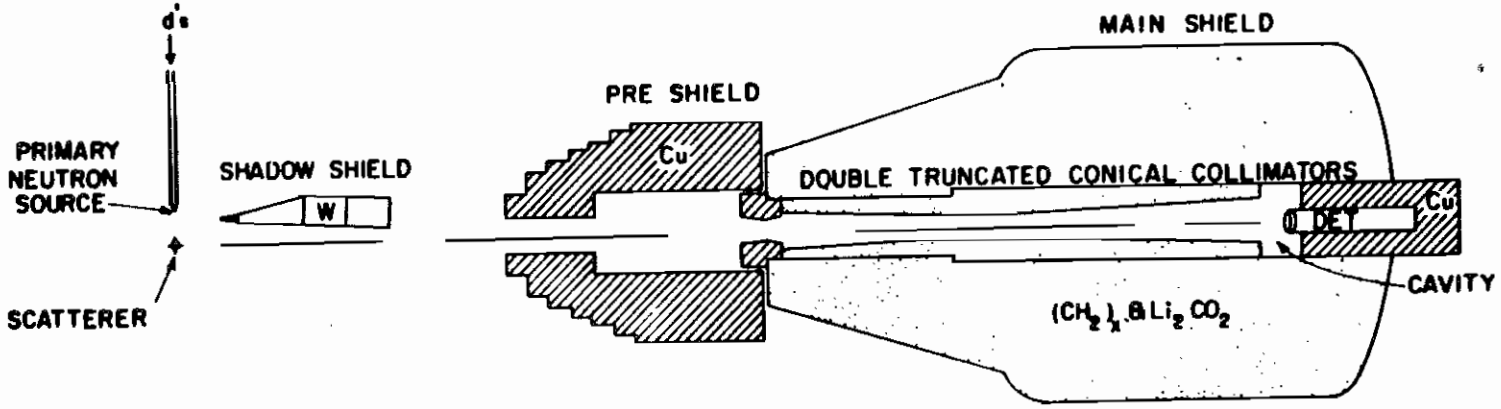
d's
PRIMARY NEUTRON SOURCE
SCATTERER
SHADOW SHIELD
W
PRE SHIELD
Cu
MAIN SHIELD
DOUBLE TRUNCATED CONICAL COLLIMATORS
DET
Cu
CAVITY
$(CH_2)_x$ & Li_2CO_2

The shield is made of paraffin to which has been added an equal amount of lithium carbonate. The paraffin and lithium carbonate were mixed as described by Glasgow [10] to minimize settling of the lithium carbonate and the formation of voids. The collimator is a double truncated cone made of paraffin and lithium carbonate designed to eliminate neutrons scattered from the air around the sample but to allow the detector an unobscured view of the sample. The double cone form serves to minimize neutron scattering from the walls of the collimator itself. The detector is shielded from gamma rays by the lead and copper rings seen in Figure 3. The shield is mounted on a steel carriage which may be moved in a radial direction. The minimum flight path is 2.4 meters, and the maximum flight path is 5.7 meters. (This detector is afterwards referred to as the six meter detector; the other one is referred to as the four meter detector.)

The detector is shielded from direct-source neutrons by a massive (150 kg.) tungsten shadow bar. This shadow bar is mounted on a stand which, through the use of a carefully designed guide piece, enables the shadow bar to be optimally placed for each angle. The optimum placement was derived analytically by L.W. Seagondollar [11].

It was found on first use of the six-meter detector that there was an extraneous group of neutrons with a time-of-

flight slightly greater than that of the prompt neutrons (see Figure 4). That this group of neutrons was due to insufficient collimation of the detector was demonstrated by the addition of further collimation in the form of the copper pre-shield formerly used on the four-meter detector. In the second spectrum in Figure 4, it can be seen that the extraneous group of neutrons is removed. The collimator was carefully placed so as not to obscure any neutrons scattered by the sample. The collimation of the four-meter detector was not adversely affected by the removal of the pre-shield. The shield on its radial carriage, the pre-shield, and the shadow bar assembly are mounted on a precision-machined angular carriage. This carriage can be moved from an angle of 0° with the beam line to about 160°. The carriage was designed so that even under the weight of the shield and preshield, the maximum deviation from horizontal will be 0.040 inch. The angular carriage is easily moved by means of a drive motor.

The time resolution of the two detectors may be defined in a practical way. Two neutron groups were considered to be resolved if the program GAUSSN [12] could fit them with two gaussian peaks of equal widths. A portion of the spectrum for the ^{11}B scattering sample is shown in Figure 5. On the far left

Figure 4: Spectra at En = 14 MeV, θlab = 60°. The top spectrum was taken without the extra collimation, the bottom with. A wire was at the scattering center.

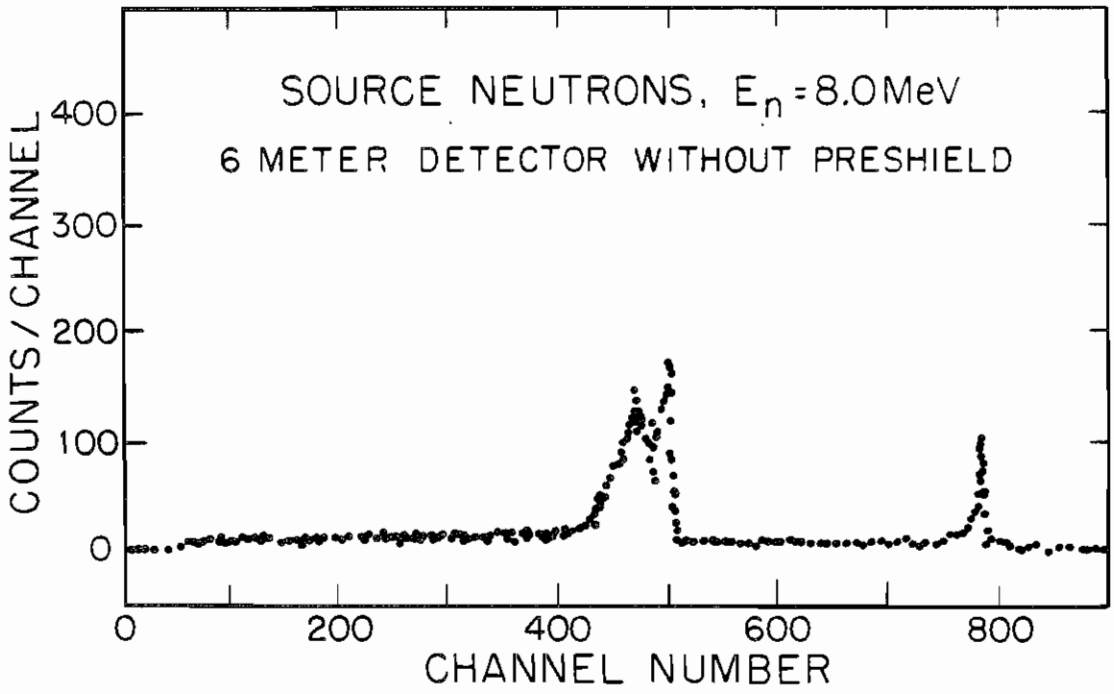
SOURCE NEUTRONS, E_n = 8.0MeV
6 METER DETECTOR WITHOUT PRESHIELD
COUNTS / CHANNEL
0
100
200
300
400
0
200
400
600
800
CHANNEL NUMBER

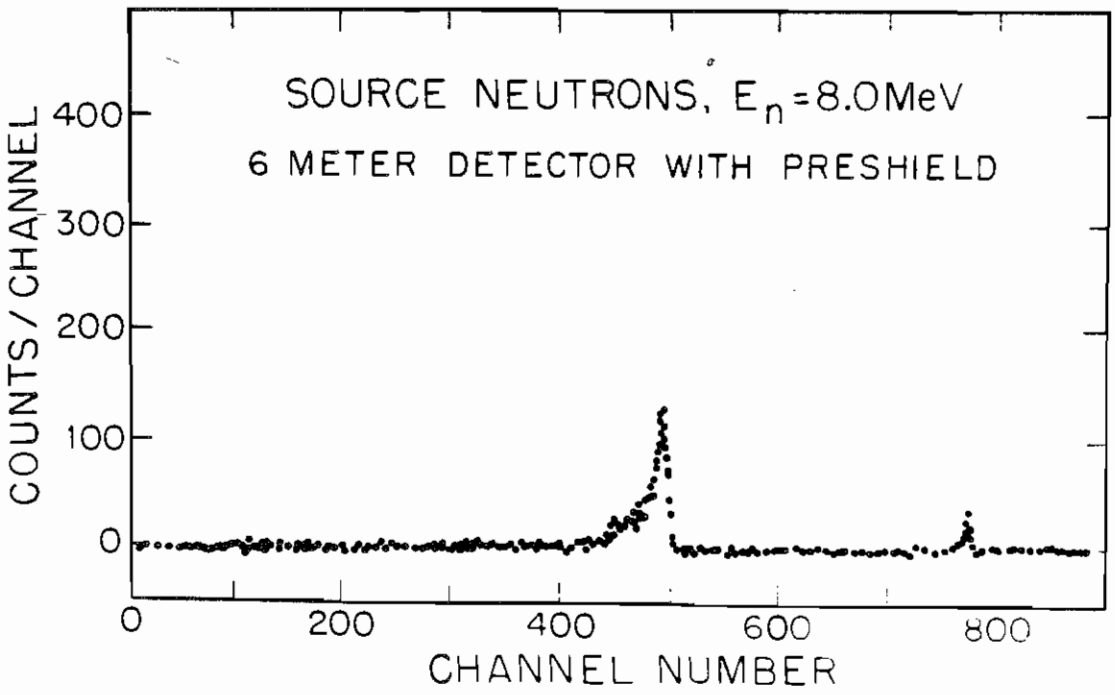
SOURCE NEUTRONS, E_n = 8.0MeV
6 METER DETECTOR WITH PRESHIELD
COUNTS / CHANNEL
0
100
200
300
400
0
200
400
600
800
CHANNEL NUMBER

Figure 5: Spectrum for neutrons scattered from ^{11}B. En = 14 MeV, θ_{lab} = 25°. The line is the fit found by the program GAUSSN (two gaussian peaks of equal width).

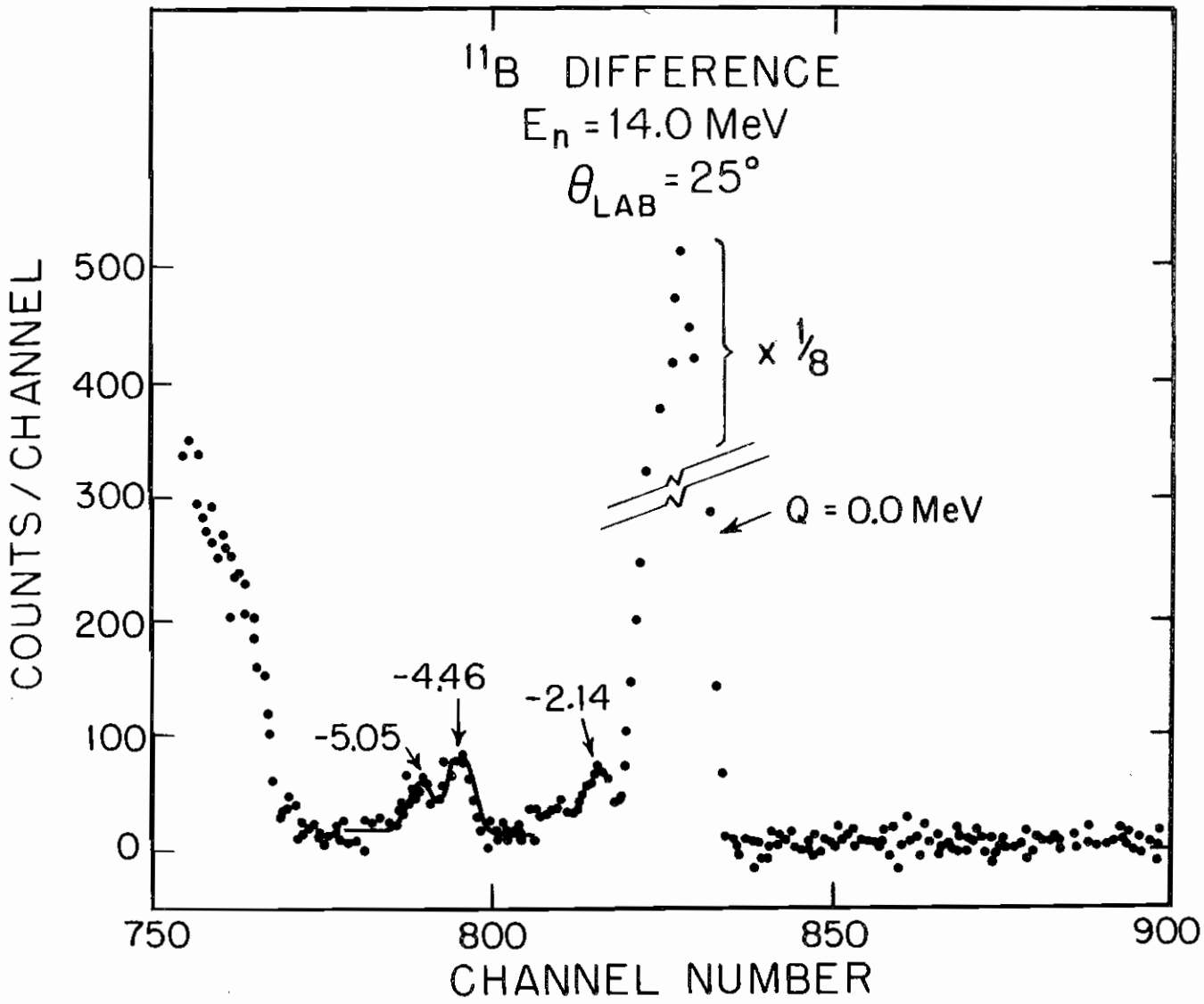
^{11}B DIFFERENCE
E_n = 14.0 MeV
θ_{LAB} = 25°
x 1/8
Q = 0.0 MeV
-4.46
-2.14
-5.05
COUNTS / CHANNEL
CHANNEL NUMBER
0
100
200
300
400
500
750
800
850
900

can be seen the beginning of the deuteron breakup group. The two peaks labelled -4.46 and -5.14 correspond to scattering to the second and third excited states of ^{11}B. The line is the fit found by the program GAUSSN. The separation between the centroids of the two peaks is about ten channels, which corresponds to a time separation of about 2.2 ns; this was the best resolution found for these data. The average energy spread of the beam was less than 0.2 MeV, giving the following expression for the energy resolution

$$\Delta E = (4 * 10^{-2} + 1.447 * 10^{-4} * E^3)^{1/2}$$

for the six-meter detector and

$$\Delta E = (4 * 10^{-2} + 3.258 * 10^{-4} * E^3)^{1/2}$$

for the four-meter detector. A plot of ΔE vs. E is shown in Figure 6.

This expression is valid if the two peaks are of comparable size. The program GAUSSN finds poor fits for two overlapping peaks if one is more than 40 times the height of the other one. In the ^{11}B spectrum shown in Figure 5, the two peaks labelled Q = 0.0 MeV and -2.14 correspond to the elastic group and the group from neutrons scattered from the first excited state. It was found that fits obtained by GAUSSN to these two states were of poor quality even though two peaks are clearly visible. The ratio between the heights of the two peaks is about 70 to 1.

Figure 6: Resolution of the four and six meter detectors.

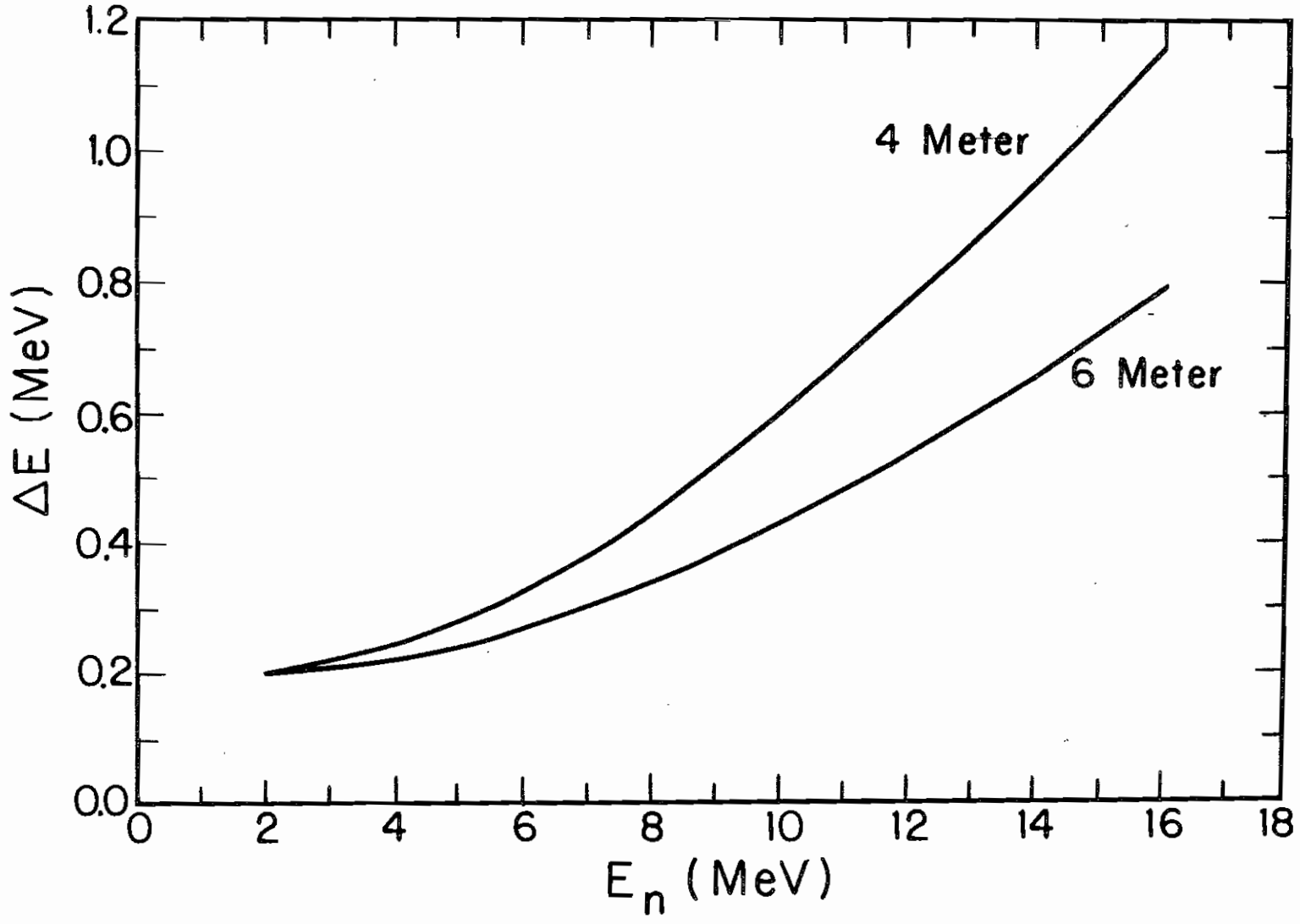
1.2
1.0
0.8
0.6
0.4
0.2
0.0
ΔE (MeV)
4 Meter
6 Meter
0
2
4
6
8
10
12
14
16
18
E_n (MeV)

Figure 7: Typical spectra for the four and six meter detectors. The scattering sample is polyethylene, En = 10 MeV, θ = 33°.

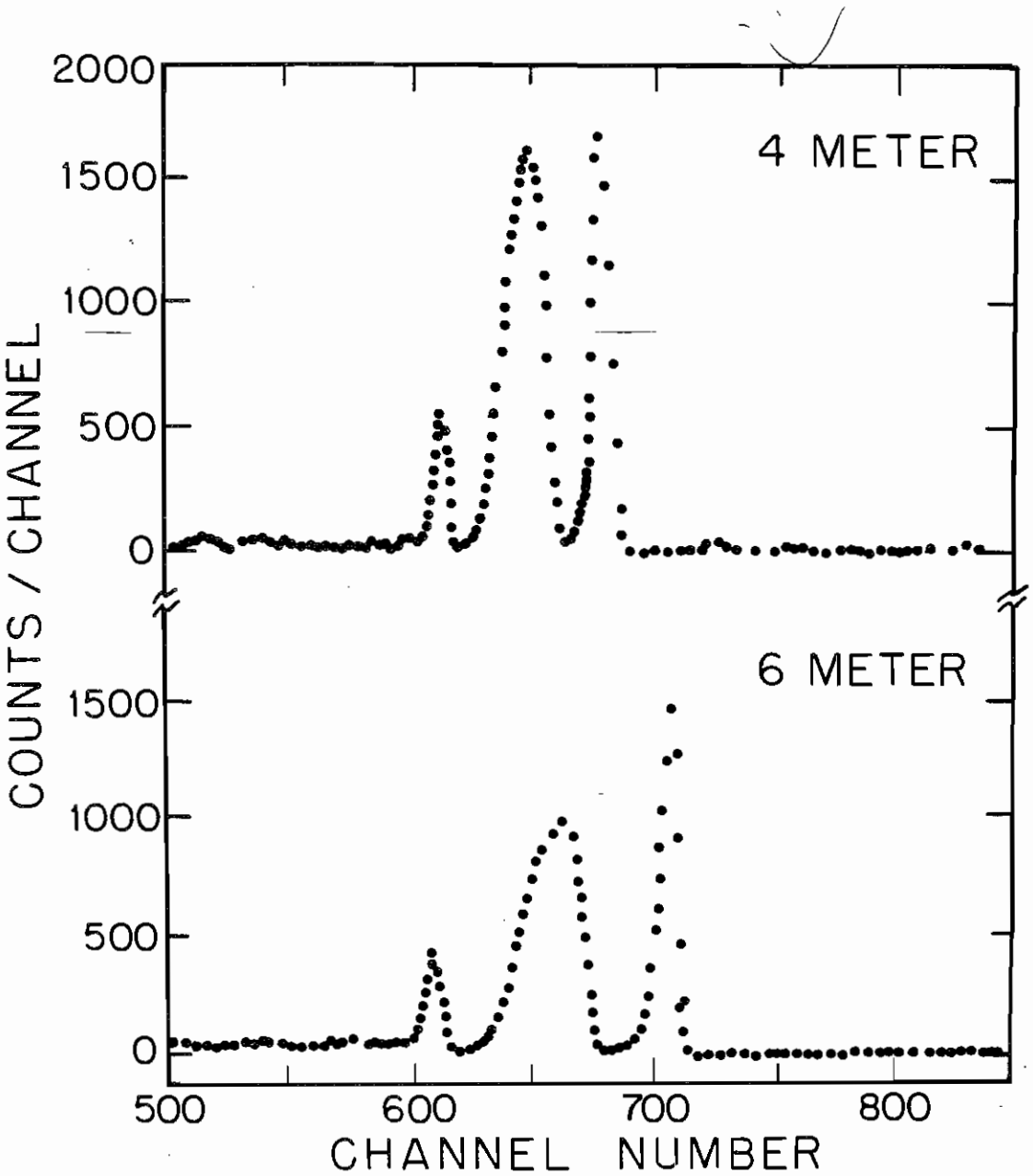
2000
1500
1000
500
0
4 METER
6 METER
1500
1000
500
0
COUNTS / CHANNEL
500
600
700
800
CHANNEL NUMBER

Typical spectra from both detectors are shown in Figure 7.

2.3 ELECTRONICS

A diagram for the electronics used for the ^{10}B data is shown in Figure 8. The setup is very similar to that shown in Hogue (1977). The only changes are in the pulse shape discrimination circuits for the three detectors. The Canberra time analyzer 1443 was substituted for the ORTEC TAC in the circuit; the Canberra time analyzer contains both a TAC and an SCA, and has the capability to generate a gate based on the setting of the SCA. Therefore, it was no longer necessary to accumulate PSD spectra while time-of-flight data were being accumulated (as had been done previously) to separate neutron signals from gamma signals. Instead, the SCA window was set around the neutron peak and the gate so generated required to be in coincidence at the computer interface with the time-of-flight signal.

Figure 8: Schematic diagram for the electronics for the three detectors.

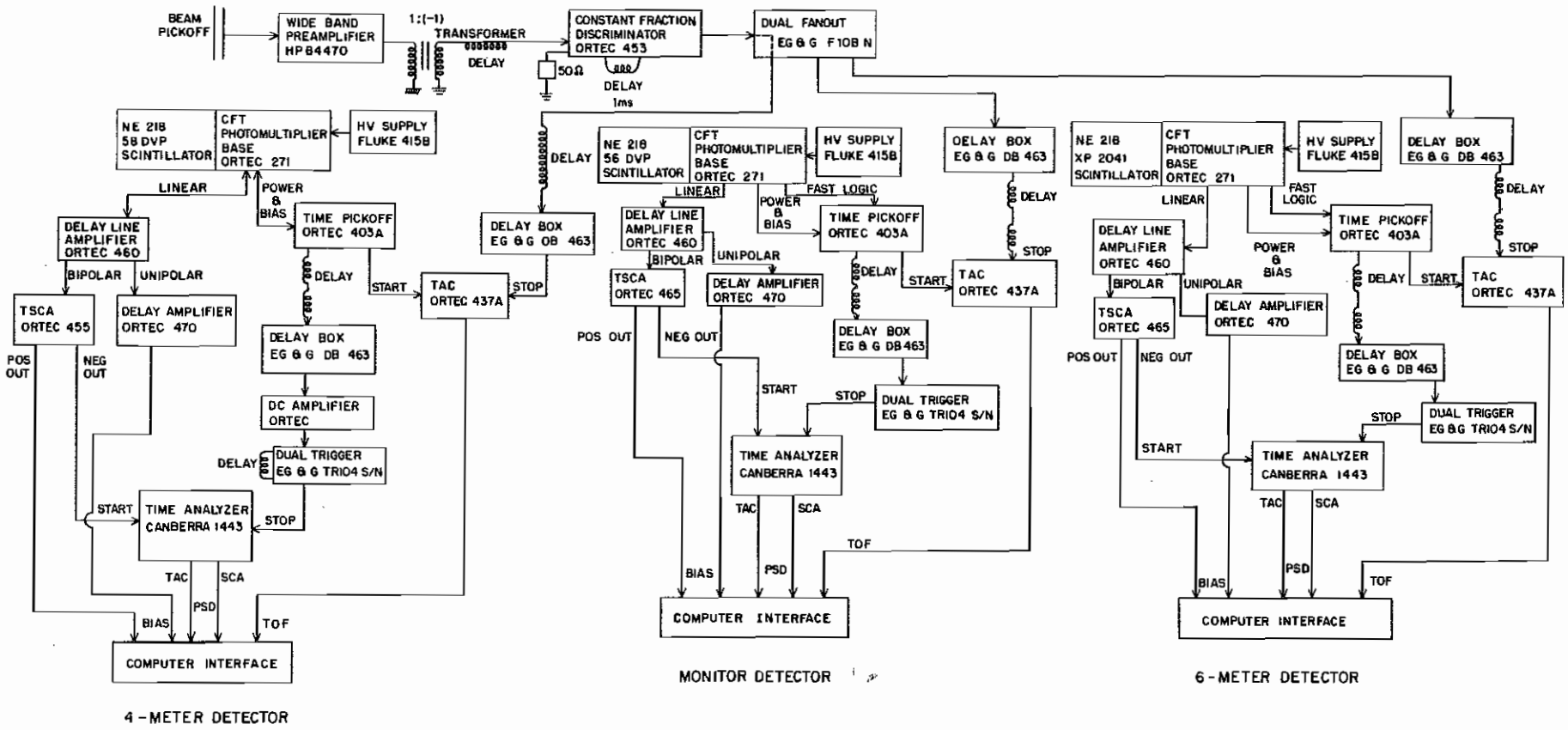
BEAM PICKOFF
WIDE BAND PREAMPLIFIER HP84470
1:(-1) TRANSFORMER
DELAY
CONSTANT FRACTION DISCRIMINATOR ORTEC 453
50Ω
DELAY
1ms
DUAL FANOUT EG&G F10B N
NE 218 58 DVP SCINTILLATOR
CFT PHOTOMULTIPLIER BASE ORTEC 271
HV SUPPLY FLUKE 415B
LINEAR
POWER & BIAS
TIME PICKOFF ORTEC 403A
DELAY LINE AMPLIFIER ORTEC 460
BIPOLAR
UNIPOLAR
TSCA ORTEC 455
DELAY AMPLIFIER ORTEC 470
POS OUT
NEG OUT
DELAY
START
TAC ORTEC 437A
STOP
DELAY BOX EG&G DB 463
DC AMPLIFIER ORTEC
DELAY
DUAL TRIGGER EG&G TRIO4 S/N
START
TIME ANALYZER CANBERRA 1443
STOP
TAC
SCA
BIAS
PSD
TOF
COMPUTER INTERFACE
4-METER DETECTOR
DELAY BOX EG&G DB 463
NE 218 56 DVP SCINTILLATOR
CFT PHOTOMULTIPLIER BASE ORTEC 271
HV SUPPLY FLUKE 415B
LINEAR
FAST LOGIC
POWER & BIAS
TIME PICKOFF ORTEC 403A
DELAY LINE AMPLIFIER ORTEC 460
BIPOLAR
UNIPOLAR
TSCA ORTEC 465
DELAY AMPLIFIER ORTEC 470
POS OUT
NEG OUT
DELAY
START
TAC ORTEC 437A
STOP
DELAY BOX EG&G DB463
START
STOP
DUAL TRIGGER EG&G TRIO4 S/N
TIME ANALYZER CANBERRA 1443
TAC
SCA
TOF
BIAS
PSD
COMPUTER INTERFACE
MONITOR DETECTOR
OELAY BOX EG&G DB 463
DELAY
STOP
NE 218 XP 2041 SCINTILLATOR
CFT PHOTOMULTIPLIER BASE ORTEC 271
HV SUPPLY FLUKE 415B
DELAY BOX EG&G DB 463
LINEAR
FAST LOGIC
DELAY LINE AMPLIFIER ORTEC 460
POWER & BIAS
TIME PICKOFF ORTEC 403A
DELAY
START
TAC ORTEC 437A
STOP
BIPOLAR
UNIPOLAR
TSCA ORTEC 465
DELAY AMPLIFIER ORTEC 470
POS OUT
NEG OUT
DELAY BOX EG&G DB 463
STOP
DUAL TRIGGER EG&G TRIO4 S/N
START
TIME ANALYZER CANBERRA 1443
TAC
SCA
BIAS
PSD
TOF
COMPUTER INTERFACE
6-METER DETECTOR

An electronic bias corresponding to a neutron energy of 2 MeV was set by disallowing signals which fell below the Compton edge energy for the gamma rays from ^{137}Cs. This bias was checked every twenty-four hours to monitor electronic drift. At this time the PSD window settings were also checked.

2.4 SAMPLES

All samples used were in the form of right circular cylinders, suspended from thin stainless steel wires. The samples were positioned with the cylindrical axis oriented vertically at a distance of 8.0 cm. from the center of the gas cell. For the oxygen data, two samples were used. The "in" sample was made of BeO with aluminum end caps. Beryllium oxide is an amorphous solid which is not hygroscopic and does not crumble, so it was not necessary to enclose it in an aluminum can. However, drilling a hole of correct diameter to insert a wire would have been too difficult, so the wire necessary to support the sample was attached to the aluminum end caps. The "out" sample was a cylinder of beryllium metal which had the same number of beryllium nuclei as the BeO sample. Aluminum end caps of the same mass as those used for the BeO sample were attached to the beryllium sample.

The two boron samples were enclosed in aluminum cans because of the tendency of the boron metal to crumble and

break apart. For the "out" spectra, aluminum cans of the same mass as those used to encapsulate the boron samples were used.

Three different samples of polyethylene were used as normalization samples (see below). Physical data on all seven samples plus the empty aluminum cans are given in Table 2.

TABLE 2

Physical Data for the Scattering Samples

Sample	Radius (cm)	Height (cm)	Aluminum C=can, EC=end cap	Mass (g)	Principal Contaminant
BeO	0.93	2.54	EC, m=0.72 g	19.19	
Be	0.67	2.68	EC, m=0.72 g	6.91	
^{10}B	0.95	2.54	C, m=2.19 g	8.65	7.59% ^{11}B
Aluminum can (used with ^{10}B)	0.95	2.54	-	2.19	
^{11}B	0.95	2.06	C, m=1.98 g	8.87	2.85% ^{10}B
Aluminum can (used with ^{11}B)	0.95	2.06	-	1.98	
Polyethylene (1) (used with BeO)	0.30	2.81	-	0.72	
Polyethylene (2) (used with ^{11}B)	0.28	2.37	-	0.62	
Polyethylene (3) (used with ^{10}B)	0.64	2.70	-	3.41	

2.5 EXPERIMENTAL PROCEDURE

The four - meter and the six - meter detectors were used simultaneously to accumulate data. Data were taken at ten degree intervals with each detector, usually for (lab) angles between 25° and 160°. The angle sets were five degrees apart for the two detectors; thus if the data from one detector were found to be of unacceptable quality, a complete angular distribution would still be available from the other detector.

For all samples, two spectra were accumulated at each angle. They are referred to hereafter as the "in" and the "out" spectra. The in spectrum was taken with the BeO sample for ^{16}O, with the ^{10}B sample in its aluminum can for the ^{10}B, and with the ^{11}B sample in its aluminum can for the ^{11}B. The out spectrum was taken with the Be sample for ^{16}O and with the proper empty aluminum can for the two boron isotopes. The out spectrum was accumulated for a number of counts determined by the following algorithm

$$q = \left[\frac{Mo}{Mi}\right]\left[\frac{\left(\frac{Ci}{Mi}\right) + \left(\frac{3}{2}\right)\left(\frac{Ci}{Mi}\right)^2}{\left(\frac{Co}{Mo}\right) + \left(\frac{3}{2}\right)\left(\frac{Co}{Mo}\right)^2}\right]^{1/2}$$

In the above expression, Mi and Ci refer to the number of counts in the monitor detector "in" spectrum and the four or six meter detector "in" spectrum, respectively, and Mo and

Co to the "out" spectra. The quantity q is constantly updated while the out spectra are being accumulated, and when q is greater than or equal to 1.0 for both the four and six meter detectors, data acquisition is stopped. This algorithm may be derived as follows. It is desired to divide the time available for data acquisition into two sections for the accumulation of the "in" spectrum and the "out" spectrum so that the error in the difference is minimized. Thus

$$ti + to = T$$

The counting rate in the monitor detector is independent of whether there is a sample in or not, as the monitor detector is aimed at the gas cell. Therefore,

$$\frac{Mi}{Mo} = \frac{ti}{to}$$

The number of good counts (normalized to monitor yield) is

$$N = \frac{Ci}{Mi} - \frac{Co}{Mo}$$

The error in this quantity may be derived. Since the error in each term is

$$\Delta X^2 = \Delta_i^2 \left(\frac{\partial Y}{\partial X}\right)^2$$

the error in the sum is

$$\Delta N = \left\{Mi * \left(\frac{-Ci}{Mi^2}\right)^2 + Ci * \left(\frac{1}{Mi}\right)^2 + Mo * \left(\frac{-Co}{Mo^2}\right)^2 + Co * \left(\frac{1}{Mo}\right)^2\right\}^{1/2}$$

$$= \left\{\frac{Ci^2}{Mi^3} + \frac{Ci}{Mi^2} + \frac{Co^2}{Mo^3} + \frac{Co}{Mo^2}\right\}^{1/2}$$

In order to minimize this quantity, we find $\frac{d\Delta N}{dMo}$ and

set it equal to 0.

Recalling that Mi + Mo = M, a constant

$$\frac{d\Delta N}{dMo} = \frac{1}{2}\left\{\frac{Ci^2}{Mi^3} + \frac{Ci}{Mi^2} + \frac{Co^2}{Mo^3} + \frac{Co}{Mi^2}\right\}^{-1/2} * 3\left(\frac{Ci^2}{Mi^4} + \frac{2Ci}{Mi^3} + \frac{-3Co^2}{Mo^4} + \frac{-2Co}{Mo^3}\right)$$

$$= 0 \quad , \text{ or}$$

$$\frac{Mi^2}{Mo^2} = \frac{\frac{3Ci^2}{2Mi^2} + \frac{Ci}{Mi}}{\frac{3Co^2}{2Mo^2} + \frac{Co}{Mo}}$$

Chapter III

DATA REDUCTION

3.1 DIFFERENCE YIELDS

The program NTOFA is used to calculate yields for the various peaks seen in the neutron time-of-flight spectra. The difference spectra are calculated as follows: first the in spectrum and the out spectrum are normalized to the number of neutrons accumulated in the monitor spectrum (less a polynomial background). The in and out spectra are then corrected for computer dead time, and the out spectrum is subtracted from the in. Thus for each channel

$$DIFF = TOF(IN) - FACC * TOF(OUT)$$

where

DIFF = number of counts in the difference spectrum TOF(IN) = number of counts in the "in" spectrum TOF(OUT) = number of counts in the "out" spectrum

$$FACC = \frac{Ymon(in)}{Ymon(out)} * \frac{DTItof}{DTOtof} * \frac{DTOmon}{DTImon}$$

Ymon(in), Ymon(out) are the background subtracted monitor yields DTI, DTO are the dead time correction factors for the in and out spectra.

In, out and difference spectra for ^{16}O are shown in Figure 9.

Calculating sums for the peaks, where they were completely separated from one another, was done by fitting a linear background around the peak of interest. A window containing the entire peak is set, and the program calculates the yield and the statistical error for the peak.

The statistical error on a peak in the difference spectrum is the sum (in quadrature) of the errors on the monitor in and out yields and the main in and out yields. The error on the yields in the individual spectra is taken to be $1/\sqrt{N}$, where N is the yield. The error involved in the subtraction of background is estimated as follows. The background is assumed to be a constant function of angle for a given energy. This constant is taken to be the mean of the background subtracted at all the angles. The error is then calculated as the deviation of an individual background from this mean. The background error is added in quadrature to the statistical error. This error is the relative error, to differentiate it from the scale or normalization error which will be discussed later.

In the case where the peaks to be summed are not completely separated from one another, the program NTOFA is insufficient to calculate the yields correctly. NTOFA is used to calculate the yield for the sum of the two peaks,

and the program GAUSSN is used to determine the ratio between the yields of the two peaks. The yield for one peak is then

$$Yi(\theta) = \frac{Ygaussn(\theta)i * Ytof(\theta)}{\sum_{i=1}^{2} Ygaussn(\theta)_i}$$

where

Yi(θ) = the yield for the peak i

Ytof(θ) = the yield found by NTOFA for the sum

Ygaussn(θ)i = the yield found by GAUSSN for peak i

Criteria for determining whether GAUSSN could separate two peaks were discussed earlier. It was found that at one forward angle for ^{11}B (25° at 14.0 MeV) and at all forward angles for ^{10}B (forward of about 100°) GAUSSN could not separate the elastic peak from the first excited state peak. For the ^{11}B data, an estimate was obtained for the contribution of the 2.14 MeV state in the elastic peak by fitting the yields at other angles with Legendre polynomials (in the com frame) and extrapolating to 25°. This was also done for the ^{10}B data, but since only back angles were available the fit was arbitrarily made to only second order. Plots of these second order fits are shown in Figure 11 (see Data Presentation).

Figure 9: In, out and difference spectra for ^{16}O. The top spectrum is taken with the BeO sample, the middle with the Be sample and the bottom is the calculated difference spectrum.

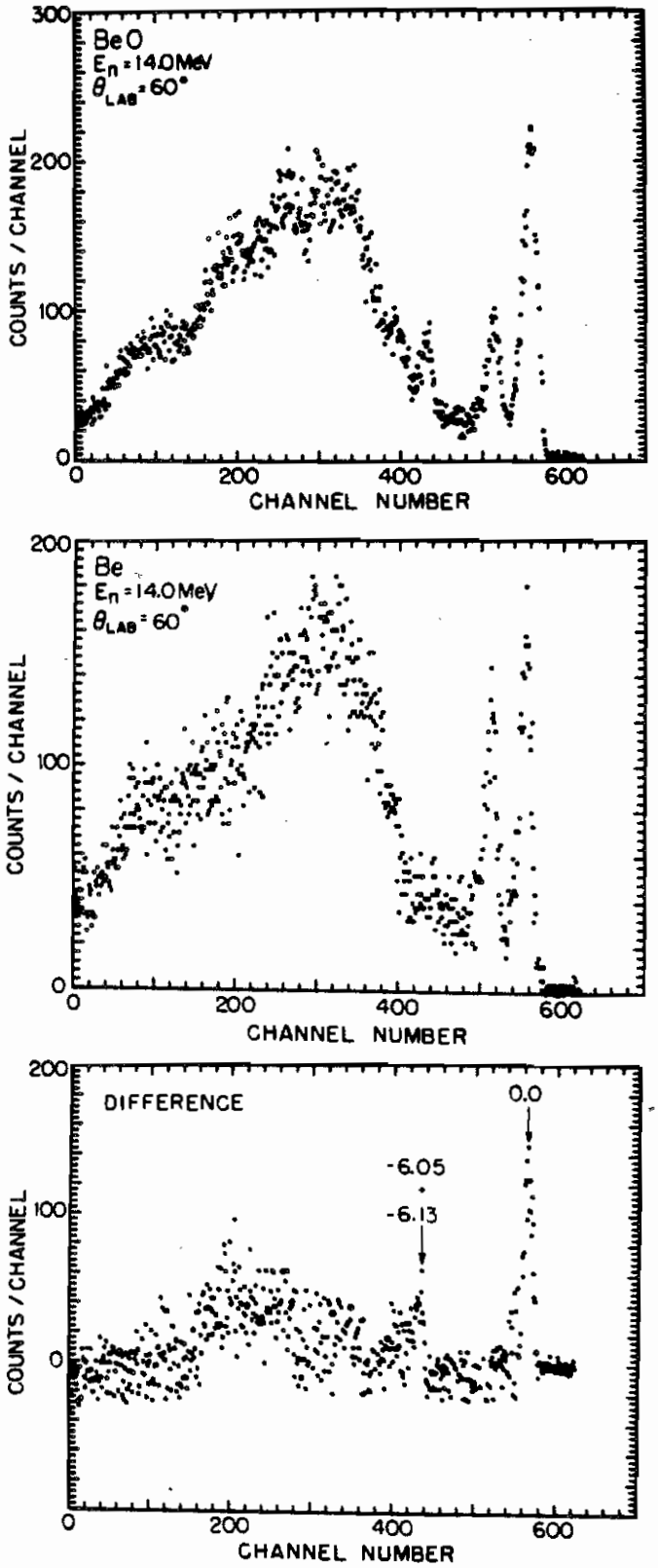
BeO
E_n = 14.0MeV
θ_{LAB} = 60°
COUNTS / CHANNEL
CHANNEL NUMBER
Be
E_n = 14.0MeV
θ_{LAB} = 60°
COUNTS / CHANNEL
CHANNEL NUMBER
DIFFERENCE
0.0
-6.05
-6.13
COUNTS / CHANNEL
CHANNEL NUMBER

3.2 NORMALIZATION

The measured differential cross sections were calculated using the equation

$$\frac{d\sigma(\theta_L, E_i)}{d\Omega} = \frac{Y_S(\theta_L)}{Y_p(\theta_p)} \cdot \frac{1}{A_p(\theta_p)} \cdot \frac{\varepsilon_p}{\varepsilon_S} \cdot \frac{n_H}{n_S} \cdot \frac{F_p}{F_S} \cdot \sigma_{np}(\theta_p)$$

where:

$\frac{d\sigma(\theta_L, E_i)}{d\Omega}$ = differential cross section for the scattering of neutrons of incident energy E_i through lab angle θ_L.

$Y_S(\theta_L), Y_p(\theta_p)$ = monitor normalized, background subtracted and dead time corrected yields for the scattering sample at θ_L and the normalization sample at θ_p.

$A_p(\theta_p)$ = attenuation correction for the polyethylene scatterer.

n_H, n_S = number of hydrogen nuclei and scattering sample nuclei in the respective samples.

$\varepsilon_p, \varepsilon_S$ = relative efficiency for the detection of neutrons of energy E_p scattered from the polyethylene and of energy E_S scattered from the scattering sample respectively.

$\sigma_{np}(\theta_p)$ = differential cross section [13] for scattering of neutrons of incident energy E_i by hydrogen through lab

angle θ_p.

F_s, F_p = fluence correction factors to correct for the fact that the scattering samples and the polyethylene scatterers are different sizes.

The height and diameter of the polyethylene normalization sample were chosen according to the criteria in Velkley [14], i.e.,

$$H_p^2(H_p^2 + D_p^2) = H_s^2(H_s^2 + D_s^2)$$

where H_p and D_p are the height and diameter of the polyethylene scatterer and H_s and D_s refer to the samples.

For the D(d,n)^{3}He cross section, if this height/diameter criterion is met, Velkley has shown that the ratio F_p/F_s = 1.0 $\pm$ 0.01. The ratio was assumed to be 1.0.

The relative efficiencies of both main neutron detectors for 2.0 < E < 15 MeV were measured using precisely determined D(d,n)^{3}He cross sections measured by Drosg and Drake [15] and Jarmie [16], and were checked with n-p scattering. Uncertainties in the D(d,n)^{3}He cross section used to determine the relative efficiency curves varied from 1.2 to 2.2%. Angular uncertainty of approximately 0.25° during the efficiency measurements contributed from 1 to 2% to the error. Counting statistics in the measurements ranged from 1 to 2% for an overall efficiency uncertainty ranging from 2.5 to 3.5%. The relative efficiency enters into the data analysis

as the ratio $\varepsilon_p / \varepsilon_s$ where ε_p is the efficiency of the detector for neutrons scattered from the hydrogen (polyethylene) normalization sample and ε_s is the efficiency for neutrons scattered from the sample of interest. The effect of uncertainties in the relative efficiency upon this ratio was investigated. A large number of efficiency curves were generated by requiring a spline fit to randomly chosen points falling within the error bars of the measured efficiency values. The ratio $\varepsilon_p / \varepsilon_s$ was calculated for each curve for varying neutron energy differences between the scattering measurement and the normalization measurement. The error in the ratio $\varepsilon_p / \varepsilon_s$ was then calculated as the RMS deviation of the distribution of values resulting from the different curves. It was found that a very good approximation to these results could be obtained as follows:

Let $| E_{normalization} - E_{sample} | = \Delta E$ (MeV)

then:

for $\Delta E > 1.0$ MeV, $\frac{\delta \varepsilon}{\varepsilon} = 2.5\%$

for $\Delta E < 1.0$ MeV, $\frac{\delta \varepsilon}{\varepsilon} = 2.5\% * (\Delta E)$

3.3 DATA CORRECTION

In the above expression, $A_p(\theta_p)$ represents the attenuation in the normalization sample. This value was calculated for all three samples using the disc approximation [17]. In this approximation

$$A_p(\theta_p) = \exp\{-[(\sigma_H(E_i)\rho_H + \sigma_C(E_i)\rho_C) * \frac{\pi}{4} + (\sigma_H(E_p)\rho_H + \sigma_C(E_C)\rho_C) * \frac{8\pi}{3}] * R\}$$

$$\frac{8}{3\pi}$$

where

$\sigma_H(E), \sigma_C(E)$ = total cross section for neutron scattering from protons and carbon at energy E.

ρ_H, ρ_C = number densities of hydrogen and carbon in polyethylene

E_i, E_C, E_p = incident neutron energy, energy of neutrons scattered from carbon and protons at θ_p

R = radius of polyethylene sample

Calculations with the program EFFIGY (see below) showed that this approximation is good for all samples to at least 2.5%. In this calculation, a correction factor which took both attenuation and multiple scattering from both elements into account was found; this is the column in Table 3 labelled "Correction". This correction factor is compared with a correction factor caluclated using the disk approximation.

The program EFFIGY is a program designed to correct neutron scattering data for the effects of extended source, large samples, and large detectors. The code is derived

TABLE 3

Results of EFFIGY Calculations for Polyethylene

Radius (cm)	Height (cm)	E (MeV)	θ (deg)	Correction (EFFIGY)	Disc Approximation	Discrepancy (%)
0.635	2.7	10.0	30.	1.186	1.175	0.9
0.295	2.8	10.0	30.	1.106	1.078	2.6
0.635	2.7	13.0	30.	1.154	1.139	1.3
0.295	2.8	13.0	30.	1.061	1.063	0.2

from an Oak Ridge program written by Kinney et al. and modified by Velkley et al. However, these programs were written to treat the relatively simple problem of scattering from samples of heavier elements which contained only one element. For that case, the following assumptions were made:

1. Kinematic energy loss by neutrons in scattering is negligible (neutrons scattered any number of times are still in the time of flight window).

2. There are no resonances in the energy region of interest.

3. The angle uncertainty due to finite size of source, sample and detector is small.

For the elements we have been studying at the energies of interest, the following are instead true:

1. Multiple scattering from light elements reduces the neutron energy to such a degree that the neutron may not be in the time of flight window.

2. There are resonances in the energy regions of interest, so the cross sections are rapidly changing with energy.

3. Our source, sample and detector sizes are such that the angle is averaged over about 10°.

It must also be mentioned that two of the scattering samples used here are multiple-element samples.

As the program EFFIGY (written by Hogue in 1978) now stands, it has the following features:

1. Energy loss from multiple scattering and angle averaging due to finite geometry are taken into account.

2. The time-of-flight spectrum is calculated using Monte Carlo methods, and the user of the program sets the time-of-flight windows as they were set in the original data analysis.

3. The spectra are calculated using a table of cross sections vs. energy and angle.

4. One or two element samples are permitted, and the subtraction of an "out" spectrum is possible.

The program employs an iterative procedure for calculating correction factors for the cross sections; this is necessary because cross sections given to the library used to calculate spectra are in fact the measured cross sections, corrected only for the effects of attenuation in the sample (estimated by the disk approximation). Therefore, the program calculates correction factors for each angle, then corrects the library distributions using these correc-

tion factors. A new time-of-flight spectrum is then calculated. Generally no more than two iterations were required to match the calculated distributions to the measured ones. This updating process was optional for a given element; for example, for the BeO sample, the beryllium cross sections were already well known (see Table 1) and were not further corrected. Cross sections for energies below those measured by us are taken from the literature [18 - 21], as were total cross sections [22 - 25]. The lowest measured angular distribution is corrected first, followed successively by the higher energies to give the program the most accurate input possible for a given energy.

The calculation process was slightly different for each of the three elements under consideration, so the differences will be discussed briefly here. For the BeO sample, two spectra were calculated for each angle, one for the BeO sample and one for the Be sample. These two spectra were subtracted to produce a difference spectrum and windows of the same width as those used in the original data analysis were used to sum the peaks in the calculated spectrum. As was mentioned above, only the oxygen cross sections in the library were revised as the program performed the iterations required.

The ^{11}B sample was capable of a more straightforward procedure. No "out" spectrum was generated (it is assumed

that the effects of the aluminum can are adequately compensated for in the experimental procedure). The procedure used for setting windows in the calculated spectrum could not be the same as described above for the experimental spectrum, in which the peaks corresponding to the second and third excited states were not well separated as the program has no facility for fitting gaussian shapes to the peaks. Therefore, the windows were set as shown in Figure 10. The only error introduced in this procedure is a slight underestimation of the multiple scattering correction required; but this is small (about a 2% discrepancy when compared with energies where the peaks were well separated) compared with the statistical errors on the data.

The scattering sample used for measuring the ^{10}B data combined the problems found in the ^{16}O data and ^{11}B data. This sample contained about 8% ^{11}B (see Table 2) and also had a first excited state which was not separated from the ground state. Corrections for these effects could however be made by the program. A library of ^{11}B cross sections was included (based on those given in this work), as well as one for the ^{10}B cross sections for the elastic and inelastic states, corrected for attenuation effects using the disk approximation. These libraries were used to generate time-of-flight spectra as described above. For the angular distributions at incident neutron energies of 8 and 9 MeV, the peaks corresponding to the ^{10}B elastic and inelastic scattering were sufficiently well separated to allow setting of

Figure 10: Time - of - flight spectrum for ^{11}B calculated using EFFIGY. En = 13 MeV, θlab = 60°. The arrows show the limits for summation of each peak.

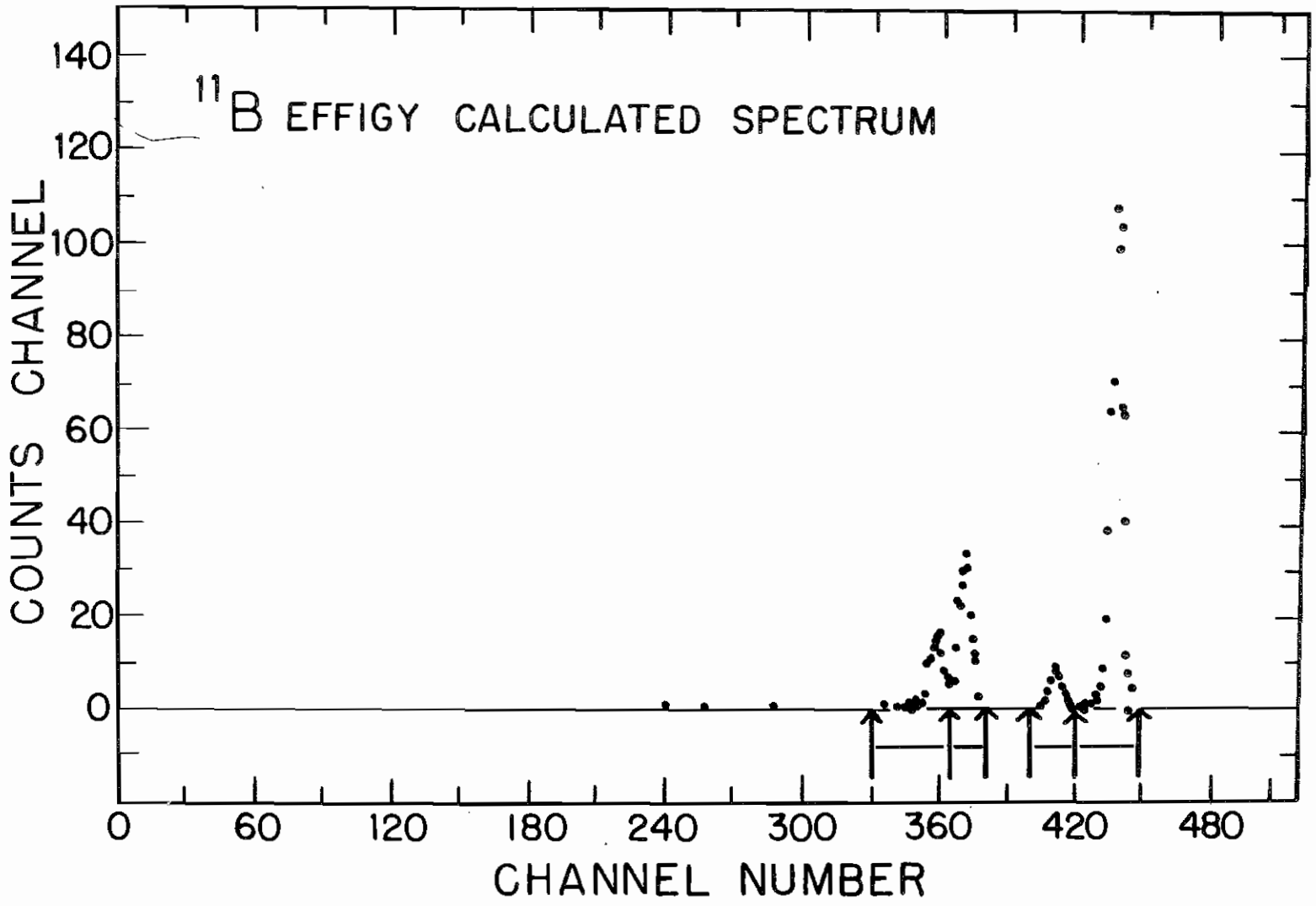
^{11}B EFFIGY CALCULATED SPECTRUM
COUNTS CHANNEL
CHANNEL NUMBER
0
20
40
60
80
100
120
140
0
60
120
180
240
300
360
420
480

two windows as was done for the ^{11}B data. The ^{10}B library cross sections were corrected iteratively as described above. At energies higher than 9 MeV, the two peaks were not well separated. Therefore, a single window was set around the double peak produced in the time-of-flight spectrum. The program was instructed to revise only the ^{10}B elastic cross section tables, as no correction factors for the inelastic cross sections could be calculated using this method; thus the only correction to the ^{10}B inelastic data at these energies was for attenuation. However, the error added by neglecting multiple scattering corrections is small compared with the statistical errors on the data.

3.4 DATA PRESENTATION

The measured ^{10}B, ^{11}B and ^{16}O angular distributions are shown in Figures 11 - 14. The solid lines shown are Legendre polynomial fits to the data. These fits were generated by a least-squares fitting routine which found the best set of coefficients a for a given order of fit, where

$$\frac{d\sigma(\theta)}{d\Omega} = \sum_{\ell=0}^{\ell_{max}} a_\ell P_\ell(\cos\theta)$$

The order chosen satisfied the following criteria:

1. The chi-squared was lower than that for the lower order fits, chi-squared being defined as usual as

$$\chi^2 = \sum_{i=1}^{N_{DATA}} \{ [\frac{d\sigma_{exp}(\theta i)}{d\Omega} - \frac{d\sigma_{calc}(\theta i)}{d\Omega}] / \Delta(\theta i) \}^2$$

where $d\sigma_{exp}(\theta i)/d\Omega$, $d\sigma_{calc}(\theta i)/d\Omega$ and $\Delta(\theta_i)$ are, respectively, the fitted cross section value, the measured cross section value, and the relative error in the measured cross section all at angle θi.

2. For the elastic distributions, the predicted zero degree cross sections must be consistent with the optical theorem, that is

$$\sigma(0^{\circ}) \geq \sigma_{WICK}$$

where

$$\sigma_{WICK} = [k\sigma_T/(4\pi)]^2$$

k = the wave number (com)

σ_T = the total neutron cross section

Figure 11: Center of mass differential cross section data for neutron scattering from ^{10}B.

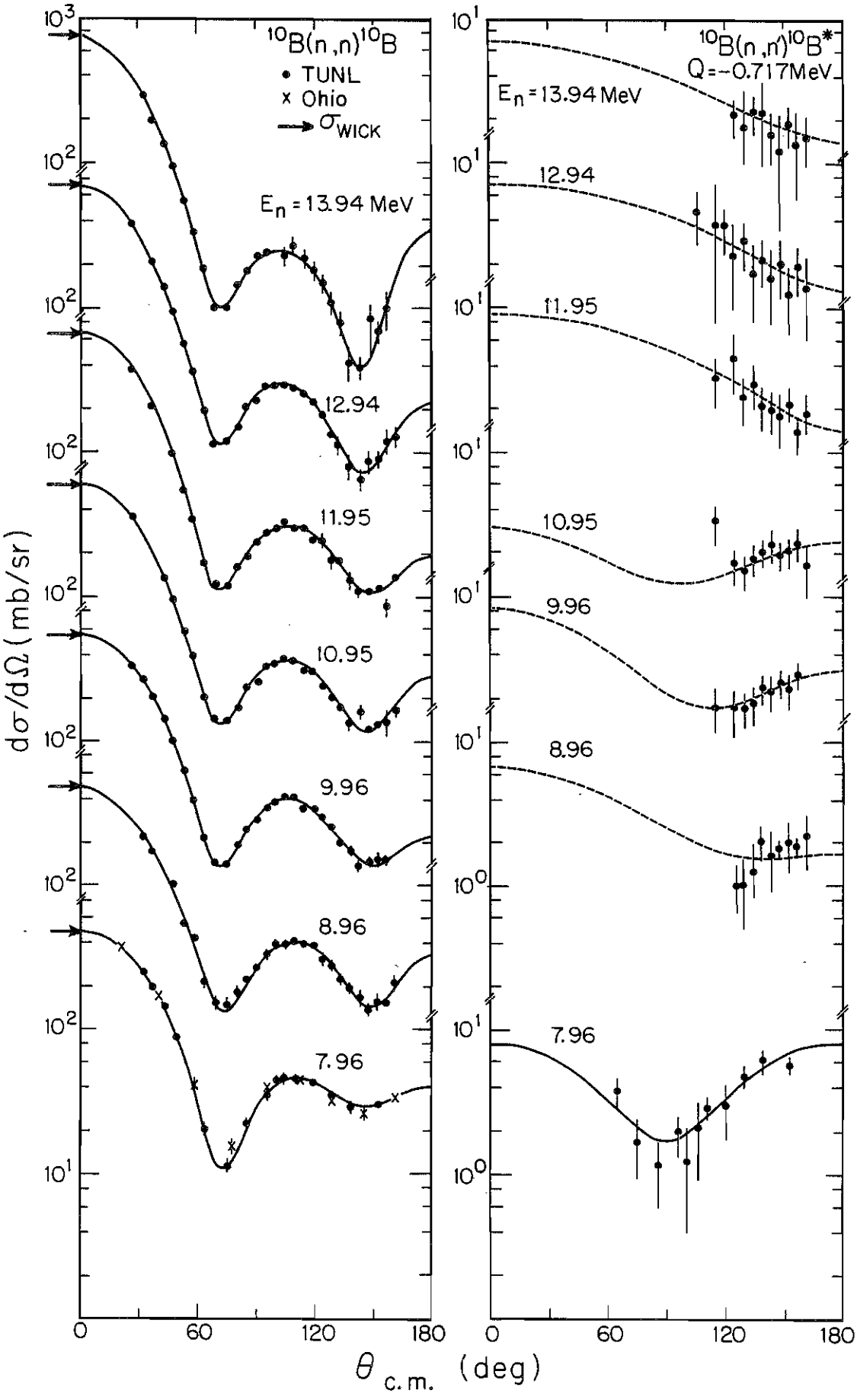
$^{10}B(n,n)^{10}B$
• TUNL
x Ohio
→ σ_{WICK}
E_n = 13.94 MeV
12.94
11.95
10.95
9.96
8.96
7.96
$^{10}B(n,n')^{10}B^*$
Q=−0.717MeV
E_n = 13.94 MeV
12.94
11.95
10.95
9.96
8.96
7.96
$d\sigma/d\Omega$ (mb/sr)
$\theta_{c.m.}$ (deg)
0
60
120
180

Figure 12: Center of mass differential cross section data for neutron scattering from ^{11}B: elastic cross sections and cross sections for scattering leaving the nucleus in the first excited state.

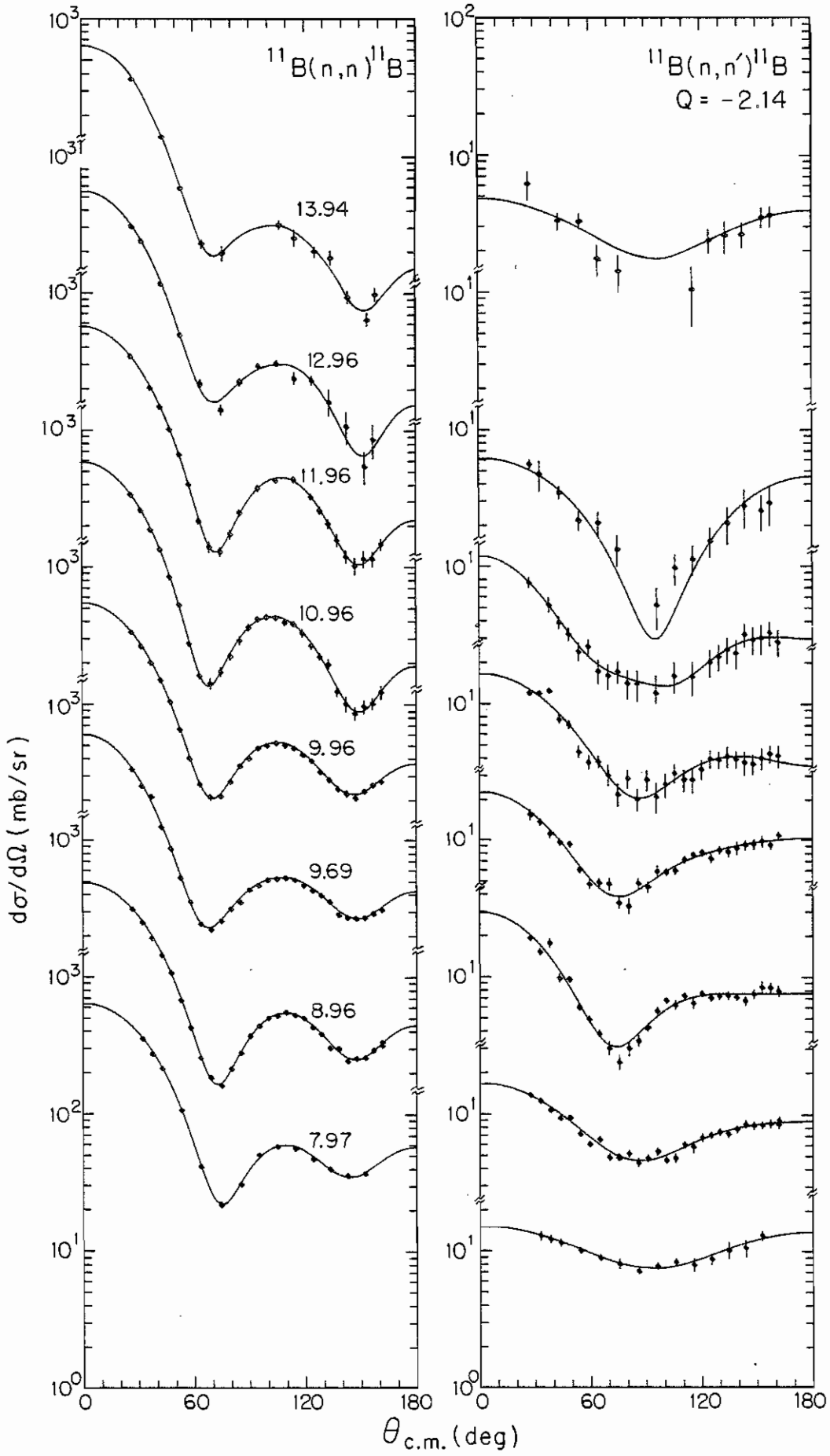
$^{11}B(n,n)^{11}B$
$^{11}B(n,n')^{11}B$
Q = -2.14
13.94
12.96
11.96
10.96
9.96
9.69
8.96
7.97
$d\sigma/d\Omega$ (mb/sr)
$\theta_{c.m.}$ (deg)
0
60
120
180

Figure 13: Center of mass differential cross section data for neutron scattering from ^{11}B: cross sections for scattering leaving the nucleus in the second and third excited states.

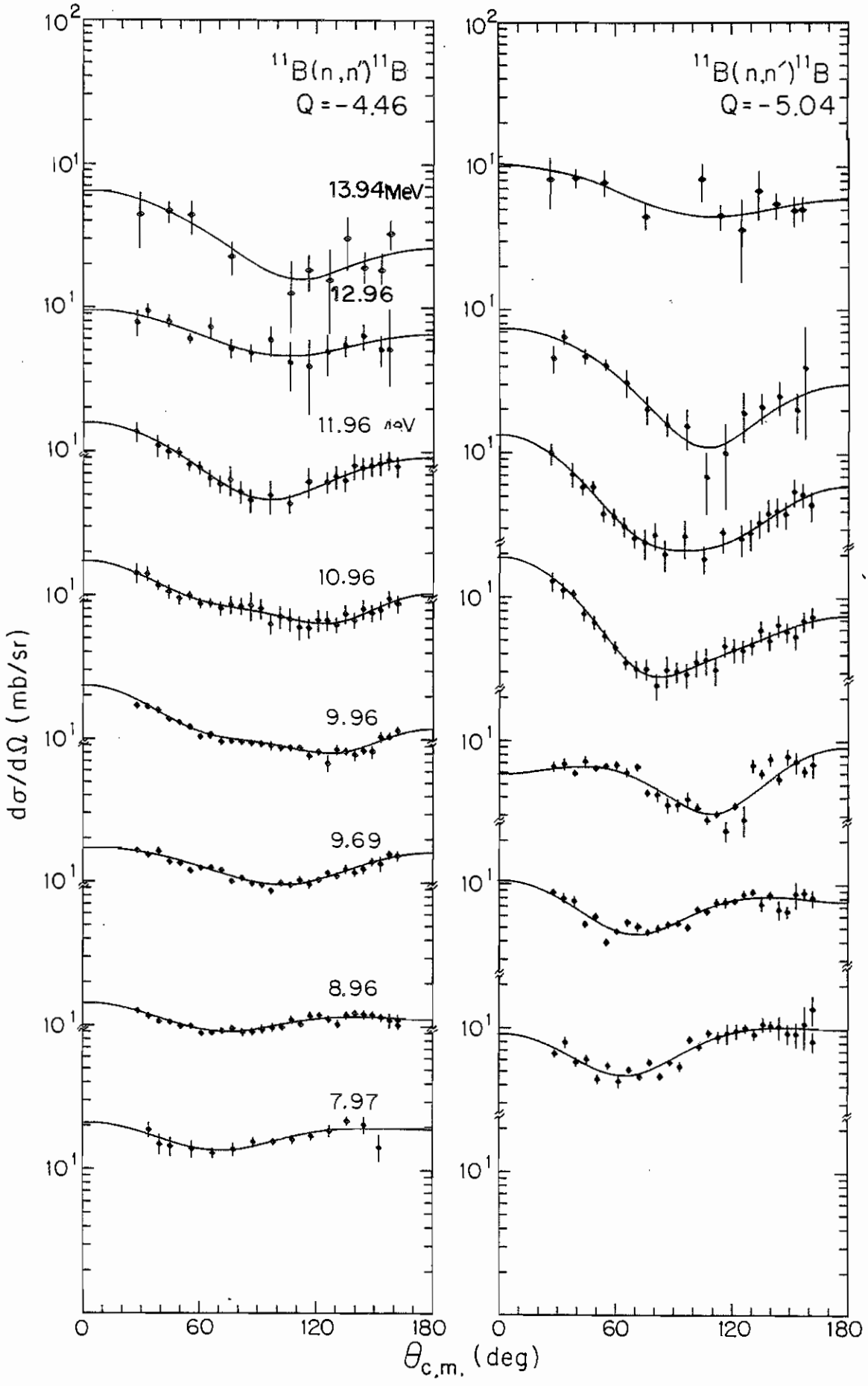
$^{11}B(n,n')^{11}B$
Q = -4.46
13.94MeV
12.96
11.96 MeV
10.96
9.96
9.69
8.96
7.97
$^{11}B(n,n')^{11}B$
Q = -5.04
$d\sigma/d\Omega$ (mb/sr)
$\theta_{c.m.}$ (deg)
0
60
120
180

Figure 14: Center of mass differential cross section data for neutron scattering from ^{16}O: elastic cross sections. The X's are small angle scattering data from Bucher et al. [26]

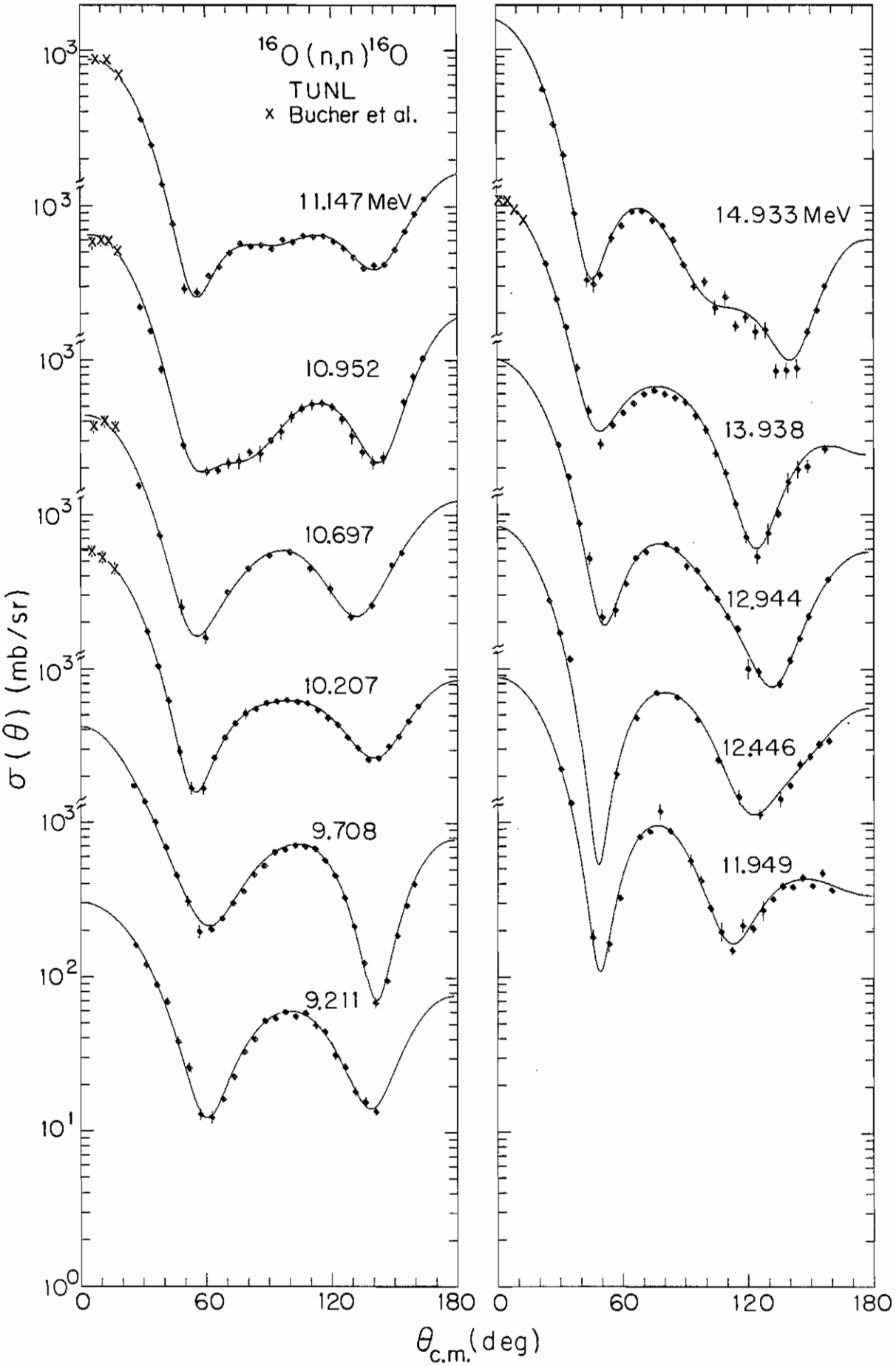
$^{16}O(n,n)^{16}O$
TUNL
x Bucher et al.
11.147 MeV
10.952
10.697
10.207
9.708
9.211
14.933 MeV
13.938
12.944
12.446
11.949
$\sigma(\theta)$ (mb/sr)
$\theta_{c.m.}$ (deg)
10^3
10^2
10^1
10^0
0
60
120
180

3. The highest order coefficient must be significant, that is, greater than the calculated error.

The dashed lines in Figure 11 are the second order fits mentioned earlier used to estimate forward angle cross section for the first excited state in ^{10}B. Data measured by White et al. (1977) for ^{10}B and ^{11}B at 8.03 MeV are included in the figures, as are data measured for small angles for ^{16}O by Bucher et al. The values for the total cross sections were taken from the ENDF/B - IV files compiled at Brookhaven National Laboratory. These total cross sections are shown in Figures 15 - 17 along with the integrated elastic and inelastic cross sections found using the above fits.

Figure 15: Neutron cross sections for ^{10}B vs. energy. The points are from the present measurements and the curves are from ENDF/B - IV.

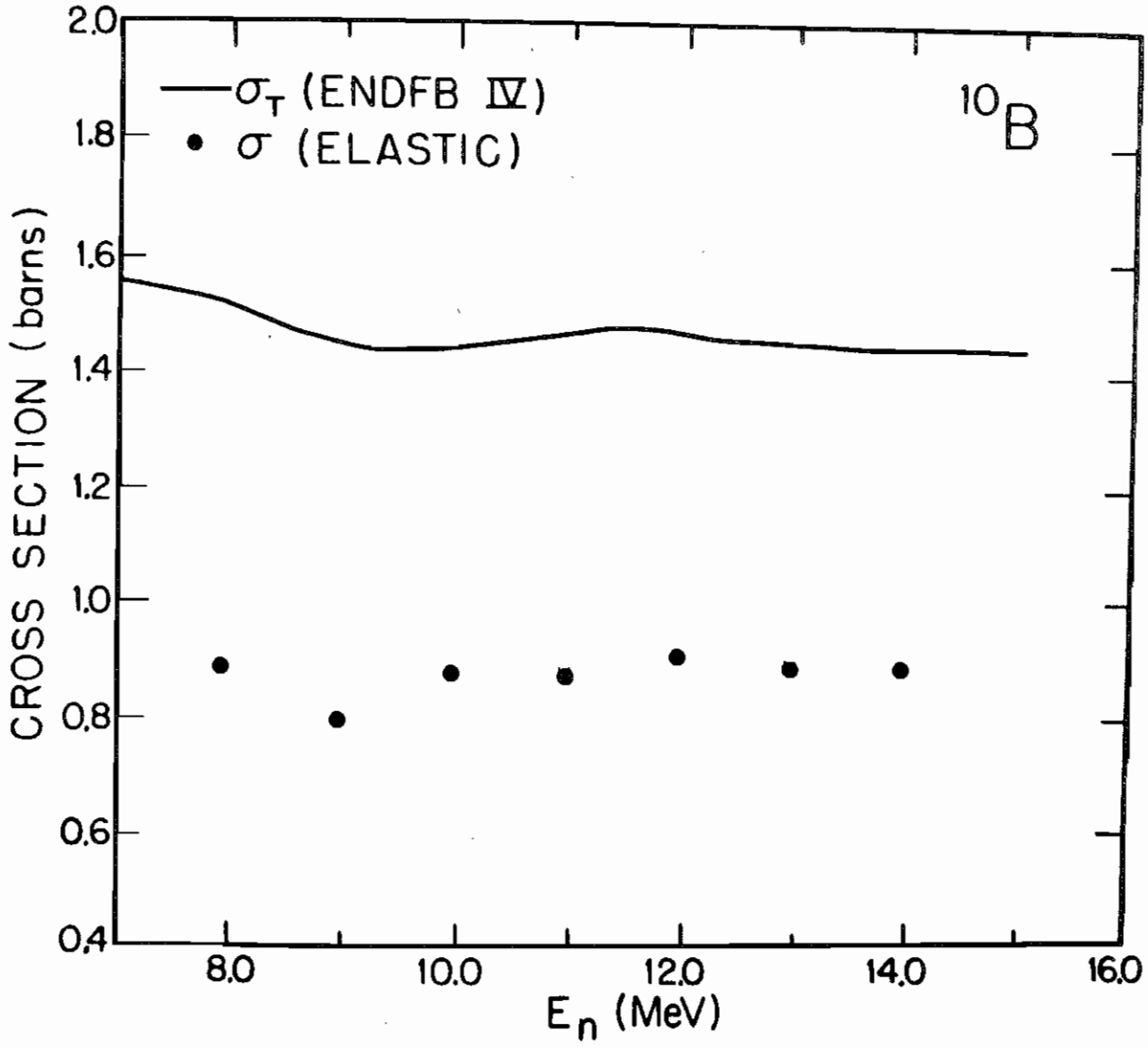
2.0
1.8
1.6
1.4
1.2
1.0
0.8
0.6
0.4
CROSS SECTION (barns)
σ_T (ENDFB IV)
σ (ELASTIC)
^{10}B
8.0
10.0
12.0
14.0
16.0
E_n (MeV)

Figure 16: Neutron cross sections for ^{11}B vs. energy. The points are from the present measurements and the curves are from ENDF/B - IV.

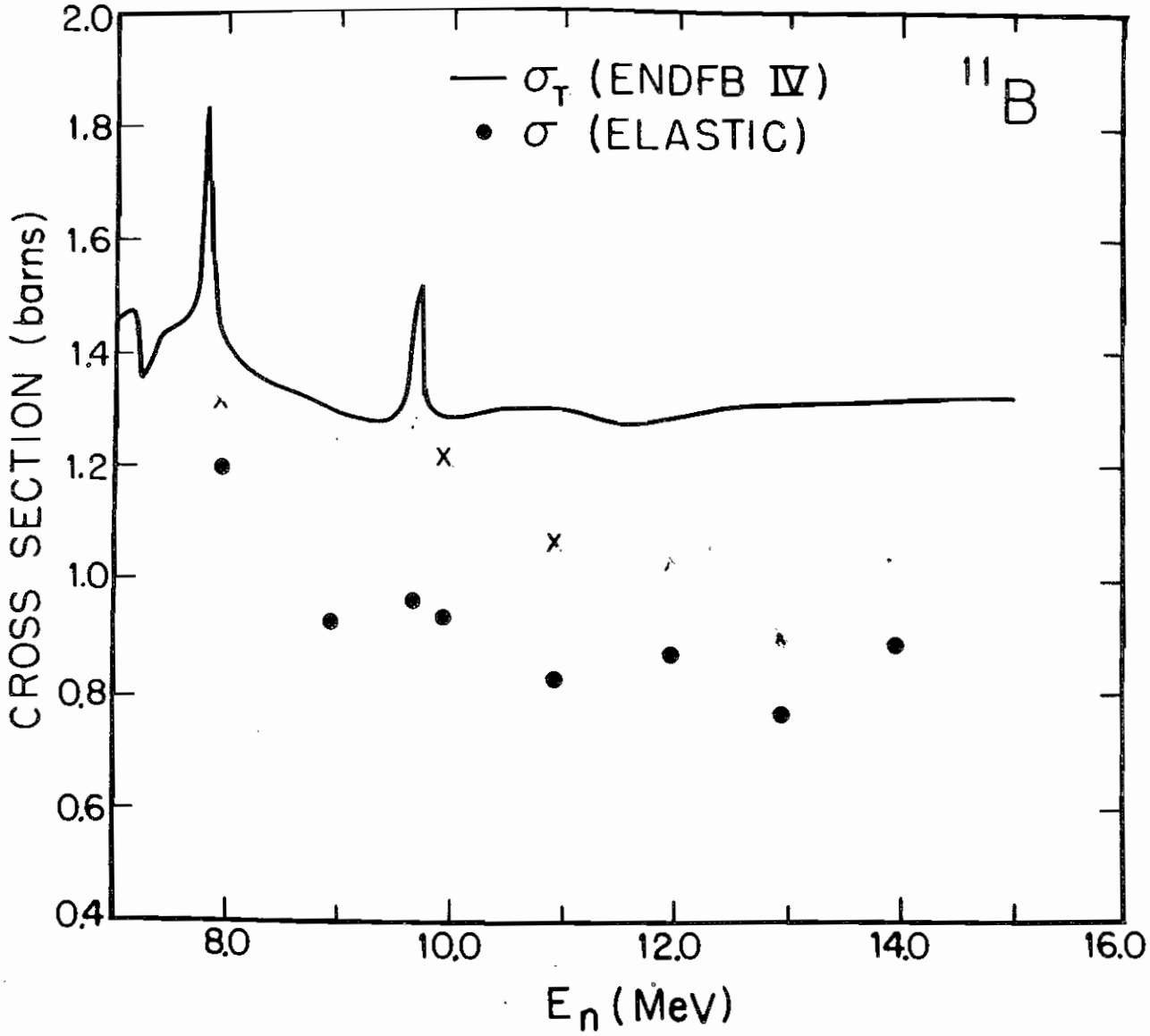
2.0
1.8
1.6
1.4
1.2
1.0
0.8
0.6
0.4
CROSS SECTION (barns)
8.0
10.0
12.0
14.0
16.0
E_n (MeV)
σ_T (ENDFB IV)
σ (ELASTIC)
^{11}B

Figure 17: Neutron cross sections for ^{150} vs. energy. The points are from the present measurements and the curves are from ENDF/B - IV.

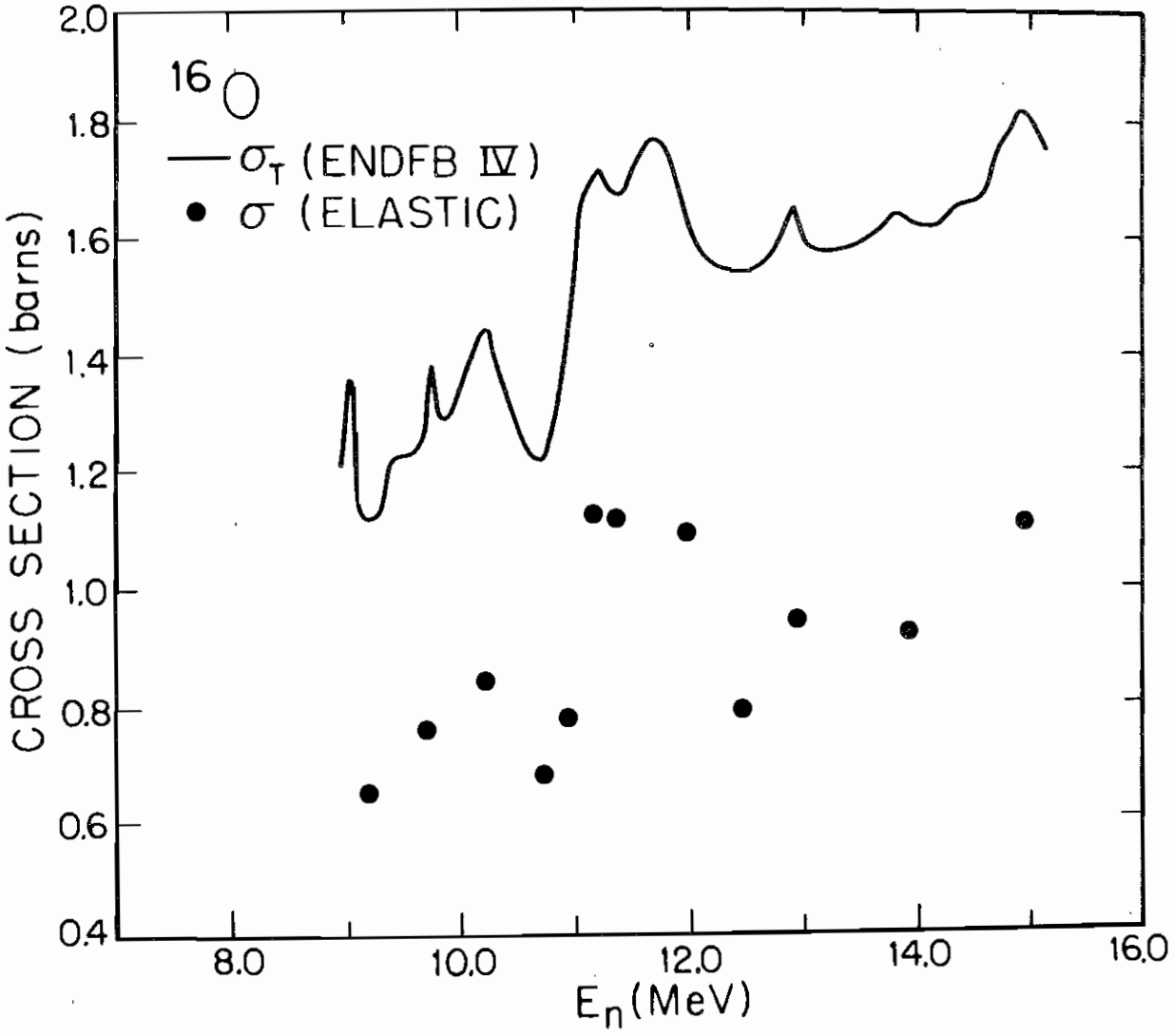
^{16}O
σ_T (ENDFB IV)
σ (ELASTIC)
CROSS SECTION (barns)
2.0
1.8
1.6
1.4
1.2
1.0
0.8
0.6
0.4
8.0
10.0
12.0
14.0
16.0
E_n (MeV)

Chapter IV

OPTICAL MODEL ANALYSES

The neutron scattering data presented here were analysed using the phenomenological optical model. That neutron data for light nuclei at these energies may be so analysed was demonstrated by Hogue (1977) and by Watson (1969). The spherical optical model was used to find fits to the $^{10}B(n,n)^{10}B$ data, the $^{11}B(n,n)^{11}B$ data and the $^{10}B(p,p)^{10}B$ data of Watson [27] between 8 and 14 MeV. Because this energy range fell for the oxygen data in a region of pronounced resonances, an extension of the SOM in which resonances are included was used for these data. Another extension of the SOM, the coupled - channel (CC) model, was used to fit both elastic and inelastic data for some of the data.

4.1 SPHERICAL OPTICAL MODEL ANALYSES

The potential used in the present spherical optical model parameter search was of the following form:

$$U(E,r) = -Vf(xr) - 4iWd\frac{df}{dr}(xi) - iWv\, f(xi)$$

$$+\lambda_{\pi}^{2}Vso\,(\vec{\sigma}\cdot\vec{l})\frac{1}{r}\frac{df}{dr}(xs)$$

$$-(Zze^2/2Rc)[3-(r^2/Rc^2)] \qquad \text{for } r<Rc$$

$$+\ Zze^2/r \qquad \text{for } r>Rc$$

where

$$f(xi) = [\ 1 + \exp(xi)\}\ ]^{-1}$$

$$xi = (r - riA^{1/3})/ai$$

$$\lambda_{\pi}^{2} = \left(\frac{\hbar}{M_{\pi}c}\right)^{2} = 2.000 \quad fm$$

In the above expression, the potential U(E,r) may be replaced by

$$U(E,r) = Un(E,r) + Uc(r) + Uso(r)$$

where the term Uc is the Coulomb potential above, the term Uso is the spin-orbit term above, and the term Un may be expressed as

$$Un(E,r) = Uo(E,r) + \frac{4}{A} U1(E,r)\vec{t}\cdot\vec{T}$$

where Uo and U1 are referred to as the isoscalar and isovector parts of the potential, and t and T refer to the isospin of the projectile and target, respectively. The diagonal terms of the isovector part are

$$Un(E,r) = Uo(E)f(r) \pm \delta U1(E)\frac{df}{dr}(r) + Ucf1(r)$$

where each of the terms is in general complex. This is customarily split into the real and imaginary terms as follows

$$V(E) = Vr(E) + Vs\ \frac{(N-Z)}{A} + Vc\ \frac{Z}{A^{1/3}}$$

and

$$W(E) = Wd(E) + Wv(E) + Ws\ \frac{(N-Z)}{A} + Wc$$

The term Wv(E) (the volume imaginary potential) is normally taken to be zero for neutron energies of less than 20 MeV (Watson, 1969). In the above expressions, the plus sign is to be taken for protons and the minus sign for neutrons. The terms Vs (N-Z)/A and Ws (N-Z)/A are called the symmetry terms and Vc Z/($A^{1/3}$) and Wc are correction terms for the isospin dependence of the nuclear force. However, it has been shown [28] that this isospin dependence may be expressed explicitly as a reduction in energy of an incident proton projectile (affecting any energy dependent parameter in the optical potential). The method for doing this was described by Rapaport: if the well depths V and Wd are allowed to have only a linear energy dependence, the corrections to the well depths may be expressed as

$$V(E) = V0 - \alpha\ Ecm + Vc * Z/(A^{1/3})$$

or

$$V(E) = V0 - \alpha\ (Ecm - Vc/\alpha * Z/(A^{1/3}))$$

and

$$Wd(E) = W0 + \epsilon\ Ecm + Wc$$

or

$$Wd(E) = W0 + \epsilon\ (Ecm - Vc/\alpha * Z/(A^{1/3}))$$

Thus, the correction to the well depth is a function of the slope found for the energy dependence and is related to the usual Coulomb correction parameter Vc.

The boron scattering data available provide a good set of data for determining the values of Vs, Ws and Vc, as for incident neutrons the Coulomb correction terms vanish. Thus, the only difference between the parameter sets for the $^{10}B(n,n)$ and $^{10}B(p,p)$ data should be the Coulomb correction term, and the only difference between the parameter sets for the $^{10}B(n,n)$ and $^{11}B(n,n)$ data should be the symmetry terms. It has been customary to correct only the real well depth for the effect of Coulomb repulsion of protons, but as this effect is to lower the energy of the incident protons it should be noted that the imaginary well depth is affected as well.

The global search code GENOA (by F. Perey) was used to find optical model parameter sets for the data. This code finds a best set of parameters for several sets of data. The data sets may vary over energy, target mass and/or projectile type. The dependence of the optical model parameters on these variables is determined by the user. The code finds a best set of parameters by minimizing the quantity

$$X^2 = \frac{1}{N} * wts \sum_{i=1}^{Ndata} \left(\frac{\sigma_i th - \sigma_i exp}{\Delta \sigma_i exp} \right)^2$$

the normalized chi-squared of the data set. The quantity wts is a weight assigned by the user to each data set; this is usually equal to 1 but if, for example, the normalization error on the particular data set were particularly large, the factor wts could be decreased to take this into account. If the sum of the individual weights is normalized to 1, the quantity X^2 would be expected to be 1 for a fit within the error bars on the points. The program also calculates the total cross section for neutrons, and this quantity is included in the calculated chi-squared if the user so specifies.

4.1.1 ^{10}B Data

The $^{10}B(n,n)$ and $^{10}B(p,p)$ data were analysed together. The procedure is described in detail here. First each data set of the neutron data was analysed separately to find a best set of parameters for the individual energy. The parameters were varied in the following way. The starting parameters were taken from Watson (1969) and the program was allowed to search on the real and imaginary well depths. These were then held fixed while the program searched on the geometric (radius and diffuseness for the real and imaginary wells) parameters. The well depths were searched on again, and the procedure repeated until no further improvement in the fits was seen. At no time were the spin-orbit parameters searched on.

The second part of the fitting procedure was to find a global set of geometric parameters for the neutron data. The geometric parameters found for each energy were averaged to find the best starting guess. The code was then allowed to search on the real and imaginary well depths, finding a different value for each energy. In searching for global parameters, it was decided to assign higher weights to the data at higher energies, using the factor wts described above, as the optical model is expected to have greater validity at higher energies, where single-particle interactions are less important. The factor wts was therefore set equal to

$$wts(Ei) = \sqrt{Ei} / \left(\sum_{i=1}^{Ndata} \sqrt{Ei}\right)$$

The normalization factor is introduced so that the sum of the squares of the weights will be 1. Then the well depths found were fitted with straight lines and the slope and intercept of these lines were treated as new variables to be searched on. The next part of the fitting procedure was to add the proton scattering data. Because the normalization uncertainty on the $^{10}B(p,p)^{10}B$ data was about 15% as compared with a normalization error on the neutron data of less than 5%, it was decided to assign less weight to the proton data (by a factor of 3). According to Rapaport (1977), the effect of the change in isospin from neutron to proton can be accounted for by changing the effective energy of the incident particle. That is, an incident proton would be

perceived as incident at a lower energy than an incident neutron because of the Coulomb repulsion, and this should therefore be taken into account in the calculation of energy dependent potentials. This was specifically introduced into GENOA; the program was required to find a best fit to both sets of data simultaneously with the energy shift between neutron and protons a variable parameter. (However, all parameters which varied with energy were required to have the same energy dependence for both projectiles.) It was found that an energy shift of 4.6 $\pm$ 1.4 MeV gave the best fit to the data; the results of this search are shown in Table 4 and Figure 18. The correction to the real well depth corresponds to a value for Vc of 0.66; however it should be noted that the imaginary well depth also varies with energy and should also have a correction term if the correction is applied in this manner rather than by using the energy shift method.

The total neutron cross section was calculated for each energy, and a comparison of the calculated results are shown in Figure 19. The parameters found differ considerably from those found by Watson (1969) for their global fits, but the energy range involved is considerably narrower. It may be noted that the data for the lowest energy in the $^{10}B(p,p)$ data fall noticibly higher than the fit in the region of the first minimum. That this effect is predominantly due to compound nucleus formation was demonstrated by Zwieglinski

et al. [29]. Their calculations showed that the effect diminished rapidly with energy; thus the neutron scattering data at the same incident projectile energy would show this effect to a lesser degree, as indeed seems to be the case.

4.1.2 ^{11}B Data

The $^{11}B(n,n)^{11}B$ scattering data were fit as described for the ^{10}B data, with the difference that because of the resonances near 8 MeV and 9.7 MeV (see Figure 16), these energies were not included in the fits. Also, because of electronics difficulties encountered in the acquisition of the 14 MeV angular distribution, this angular distribution was not included in the search, although the predicted fit is plotted. The fits found are shown in Figure 20, and the parameter values found are shown Table 5. The data were weighted as a function of energy as was done for the ^{10}B data. The predicted total cross section values are shown in Figure 21.

TABLE 4

Optical Model Parameters for ^{10}B

Parameter	GENOA	Watson
Vo (MeV)	48.1 - 0.3 Ecm	60.0 - 0.3 Ecm
ro (fm)	1.34	1.15 - 0.001 Ecm
ao (fm)	0.55	0.57
Wd (MeV)	0.16 + 0.78 Ecm	0.64 Ecm
ri (fm)	1.41	1.15 - 0.001 Ecm
ai (fm)	0.34	0.50
Vso (MeV)	5.5	5.5
rso (fm)	1.15	1.15 - 0.001 Ecm
aso (fm)	0.57	0.57
Vc (MeV)	0.66 + 0.2	0.4
rc (fm)	= ro	= ro

Figure 18: Spherical Optical Model fits to $^{10}B(n,n)^{10}B$ data and $^{10}B(p,p)^{10}B$ data. See Table 4 for values of parameters. The arrows are the Wick's limit cross section values.

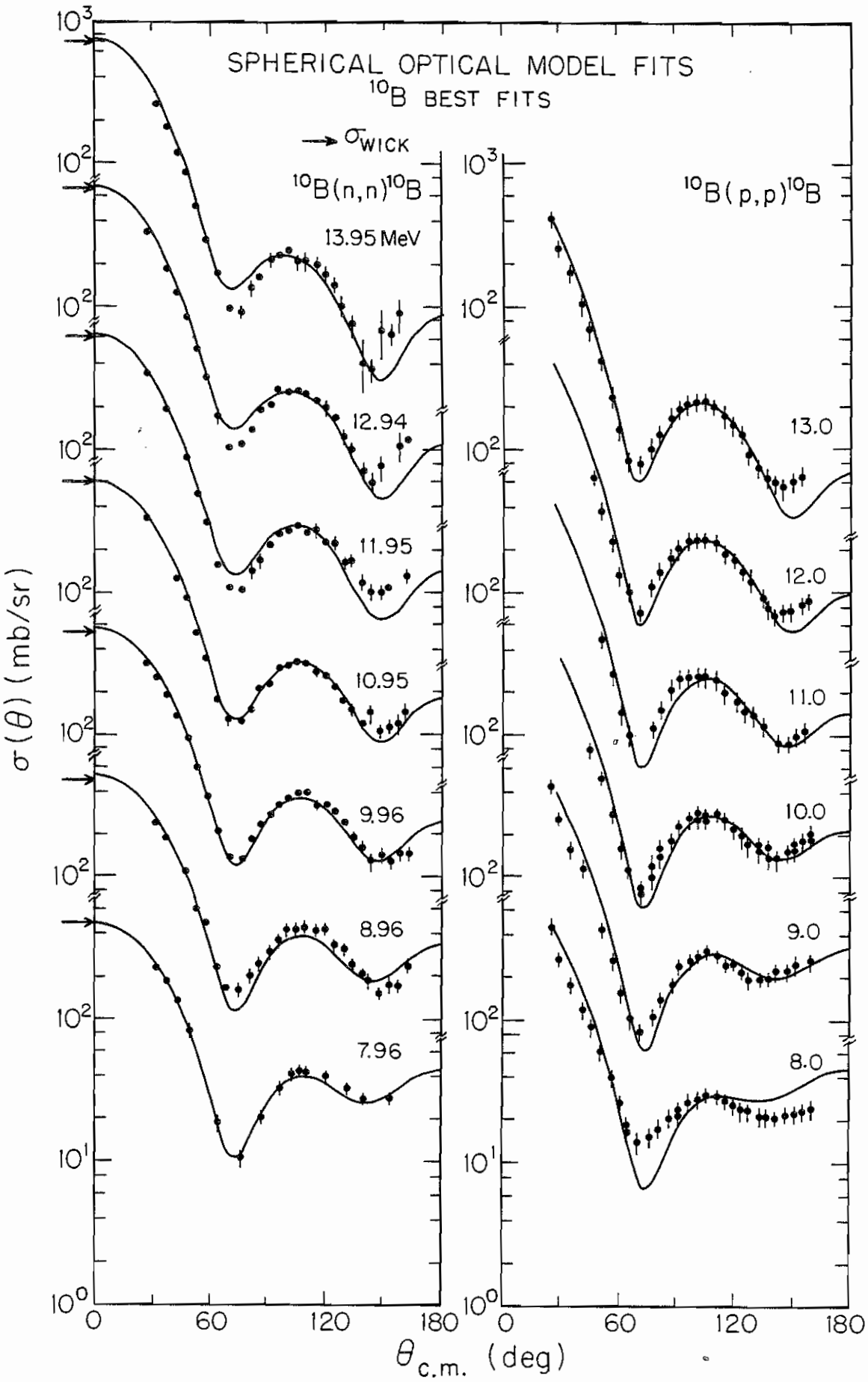
SPHERICAL OPTICAL MODEL FITS
^{10}B BEST FITS
→ σ_{WICK}
^{10}B(n,n)^{10}B
^{10}B(p,p)^{10}B
13.95 MeV
12.94
11.95
10.95
9.96
8.96
7.96
13.0
12.0
11.0
10.0
9.0
8.0
$\sigma(\theta)$ (mb/sr)
$\theta_{c.m.}$ (deg)
0
60
120
180
10^0
10^1
10^2
10^3

Figure 19: Total cross section predictions for ^{10}B. The solid line is from ENDF/B - IV. The dots are GENOA predictions from fits to ^{10}B data alone, and the circles are GENOA predictions from global fits to ^{10}B neutron and proton and ^{11}B neutron data.

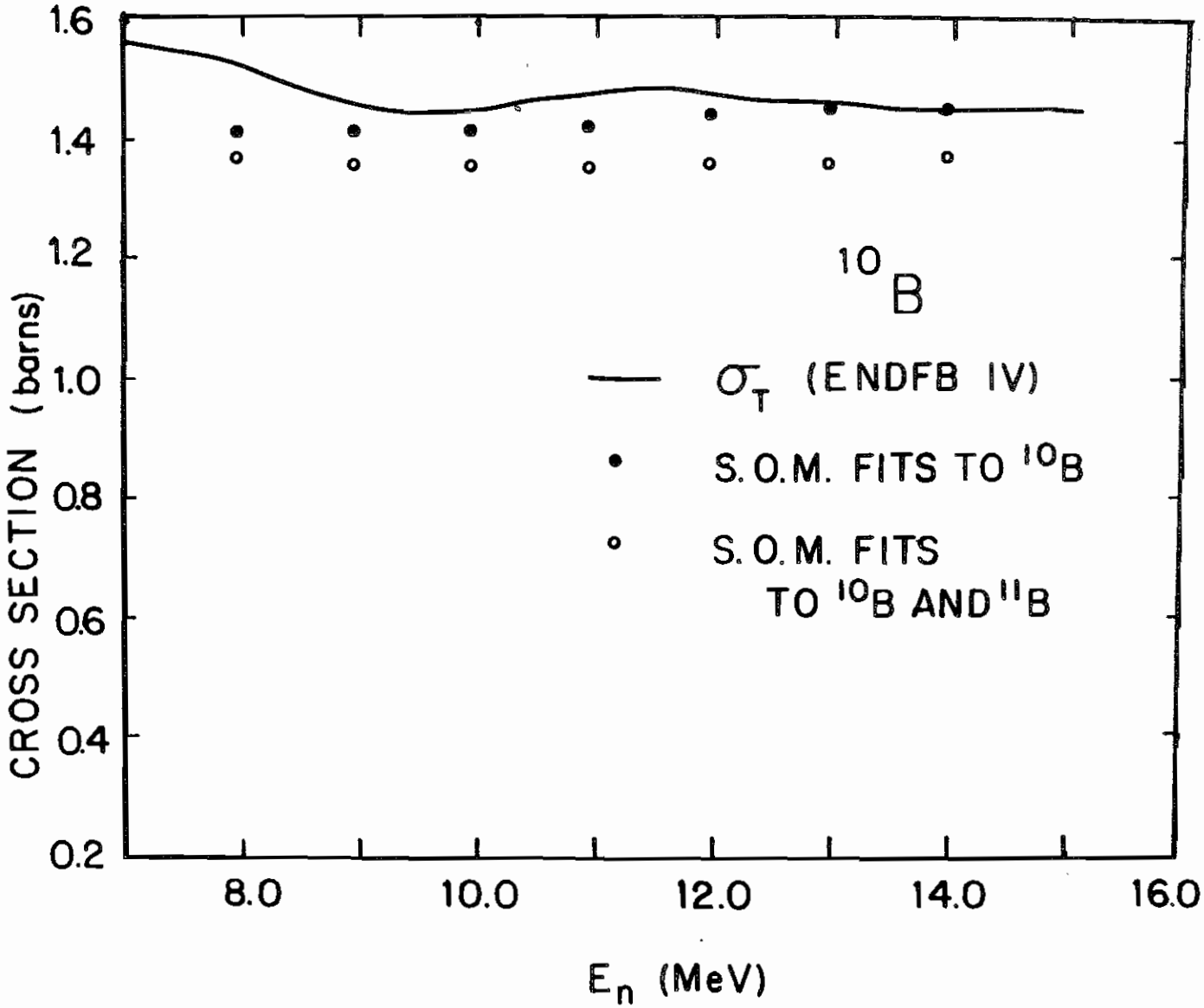
1.6
1.4
1.2
1.0
0.8
0.6
0.4
0.2
CROSS SECTION (barns)
8.0
10.0
12.0
14.0
16.0
E_n (MeV)
^{10}B
σ_T (ENDFB IV)
S.O.M. FITS TO ^{10}B
S.O.M. FITS TO ^{10}B AND ^{11}B

TABLE 5

Optical Model Parameters for ^{11}B

Parameter	GENOA	Watson
Vo (MeV)	45.7 - 0.005 Ecm	60.0 - 0.3 Ecm
ro (fm)	1.40	1.15 - 0.001 Ecm
ao (fm)	0.35	0.57
Wd (MeV)	-6.27 + 1.13 Ecm	0.64 Ecm
ri (fm)	1.10	1.15 - 0.001 Ecm
ai (fm)	0.50	0.50
Vso (MeV)	5.5	5.5
rso (fm)	1.15	1.15 - 0.001 Ecm
aso (fm)	0.57	0.57

Figure 20: Spherical Optical Model fits to $^{11}B(n,n)^{11}B$ data. See Table 5 for values of parameters. The arrows are the Wick's limit cross section values.

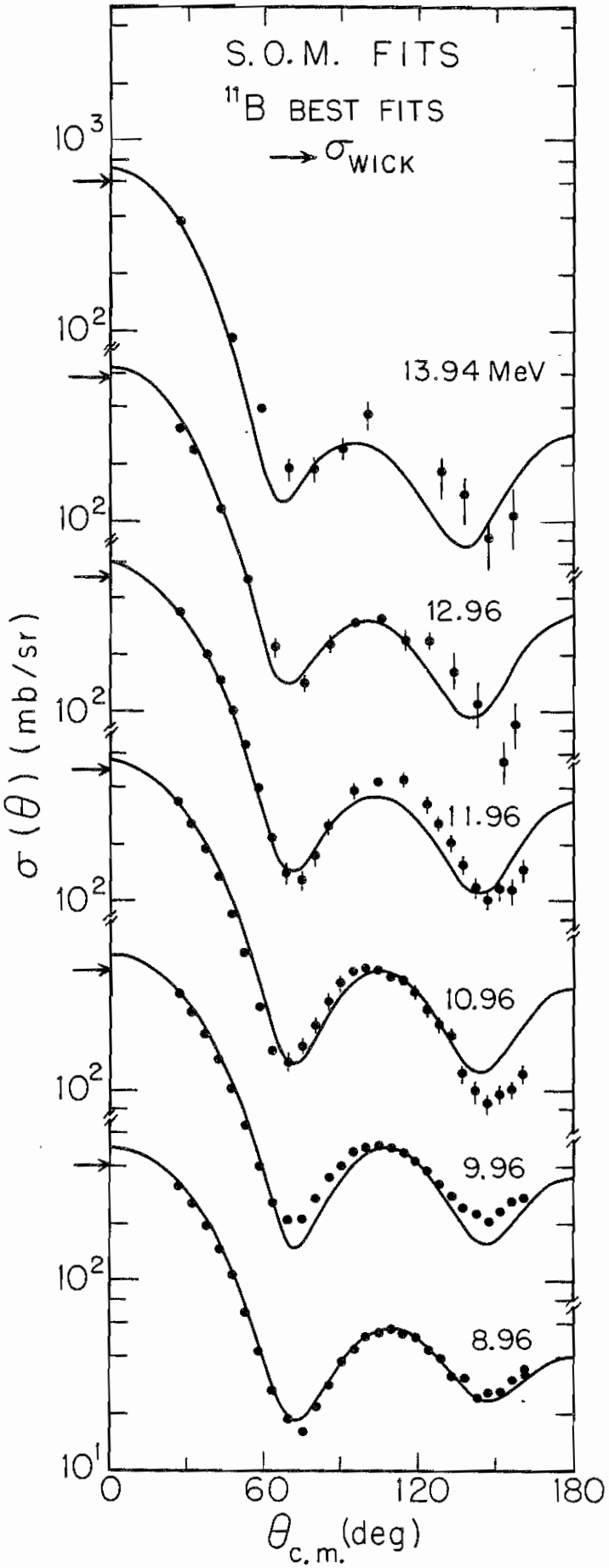
S.O.M. FITS
^{11}B BEST FITS
→ σ_{WICK}
13.94 MeV
12.96
11.96
10.96
9.96
8.96
10^3
10^2
10^1
$\sigma(\theta)$ (mb/sr)
0
60
120
180
$\theta_{c.m.}$ (deg)

Figure 21: Total cross section predictions for ^{11}B. The solid line is from ENDF/B - IV. The dots are GENOA predictions from fits to ^{11}B data alone, and the circles are GENOA predictions from global fits to ^{10}B neutron and proton and ^{11}B neutron data.

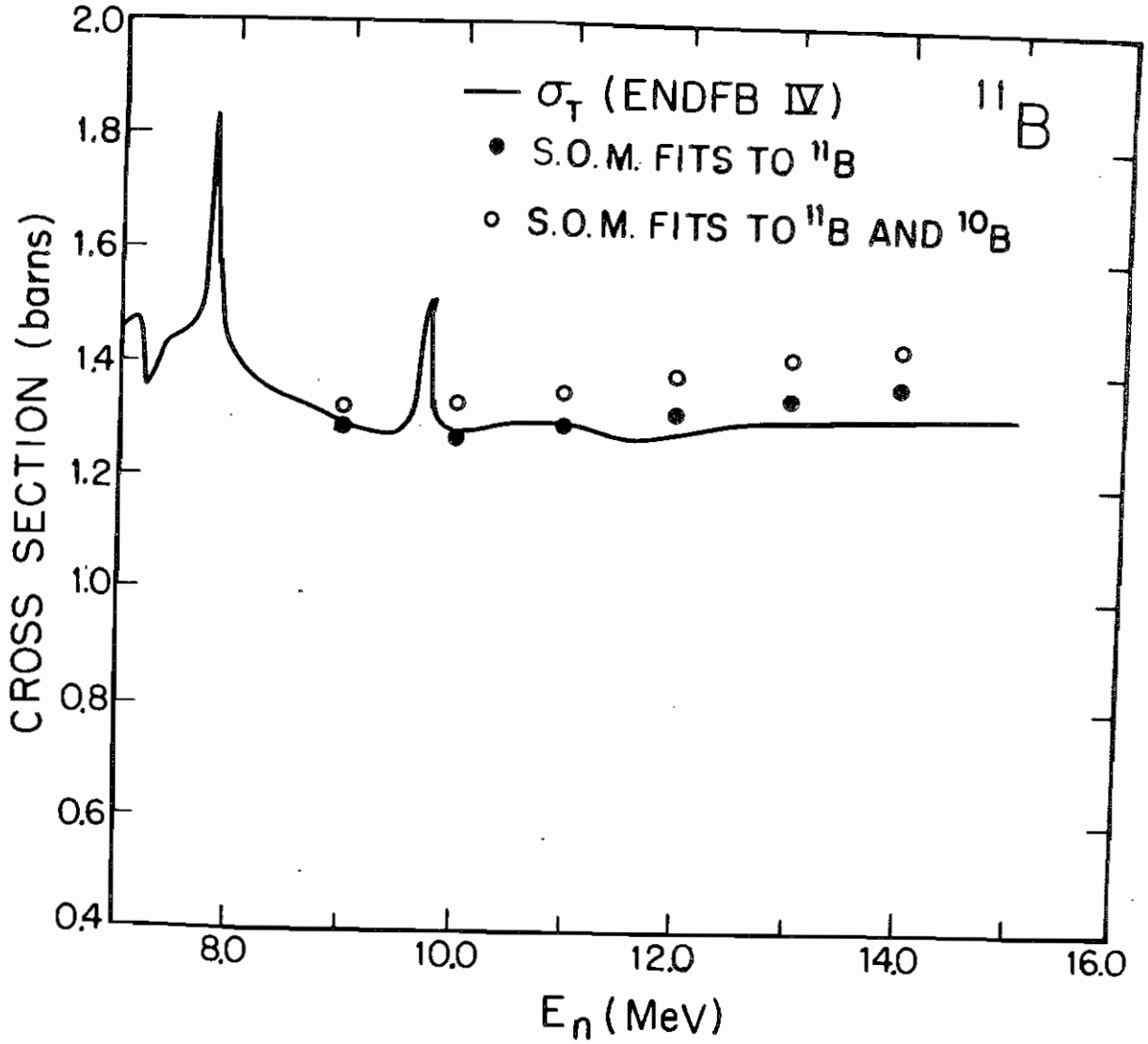
2.0
1.8
1.6
1.4
1.2
1.0
0.8
0.6
0.4
CROSS SECTION (barns)
8.0
10.0
12.0
14.0
16.0
E_n (MeV)
σ_T (ENDFB IV)
S.O.M. FITS TO ^{11}B
S.O.M. FITS TO ^{11}B AND ^{10}B
^{11}B

4.1.3 Boron Data

All of the boron data were then fit at one time. The procedure was to start with geometric parameters obtained by averaging the ^{10}B parameters and the ^{11}B parameters and, keeping these fixed, search on the best values for the slopes and intercepts of the linear fits used to calculate well depths. For this search, the value of Vc was kept at the best value found above, and the values of Vs and Ws were kept fixed at values of 24.5 MeV and 11.5 MeV, which are at about the midpoint of the range of standard values. The geometric parameters were then searched on, and the process repeated as described above. The fits so found are shown in Figure 22, and the parameters arrived at are shown in Table 6. The predicted total cross sections are shown in Figures 19 and 21.

The parameters Vs and Ws were then allowed to vary along with the well depths, and the results are the dotted curves shown in Figure 22.

TABLE 6

Optical Model Parameters for Boron Data

Parameter	GENOA	
	Standard	Best fits
Vo (MeV)	45.8 - 0.06 Ecm	45.0 - 0.06 Ecm
ro (fm)	1.37	1.37
ao (fm)	0.49	0.49
Wd (MeV)	0.05 + 0.78 Ecm	0.07 + 0.80 Ecm
ri (fm)	1.31	1.31
ai (fm)	0.33	0.33
Vso (MeV)	5.5	5.5
rso (fm)	1.15	1.15 - 0.001 Ecm
Vc (MeV)	0.66	0.66
Vs (MeV)	24.5	0.7 $\pm$ 1.0
Ws (MeV)	11.5	20.2 $\pm$ 10.0

Figure 22: Spherical Optical Model fits to $^{10}B(n,n)^{10}B$, $^{10}B(p,p)^{10}B$ and $^{11}B(n,n)^{11}B$ data. Solid lines are GENOA fits using Vs = 24.5 MeV and Ws = 11.5 MeV. Broken lines are fits using Vs = 0.7 MeV and Ws = 20.2 MeV. See Table 6 for values of parameters. The arrows are the Wick's limit cross sections.

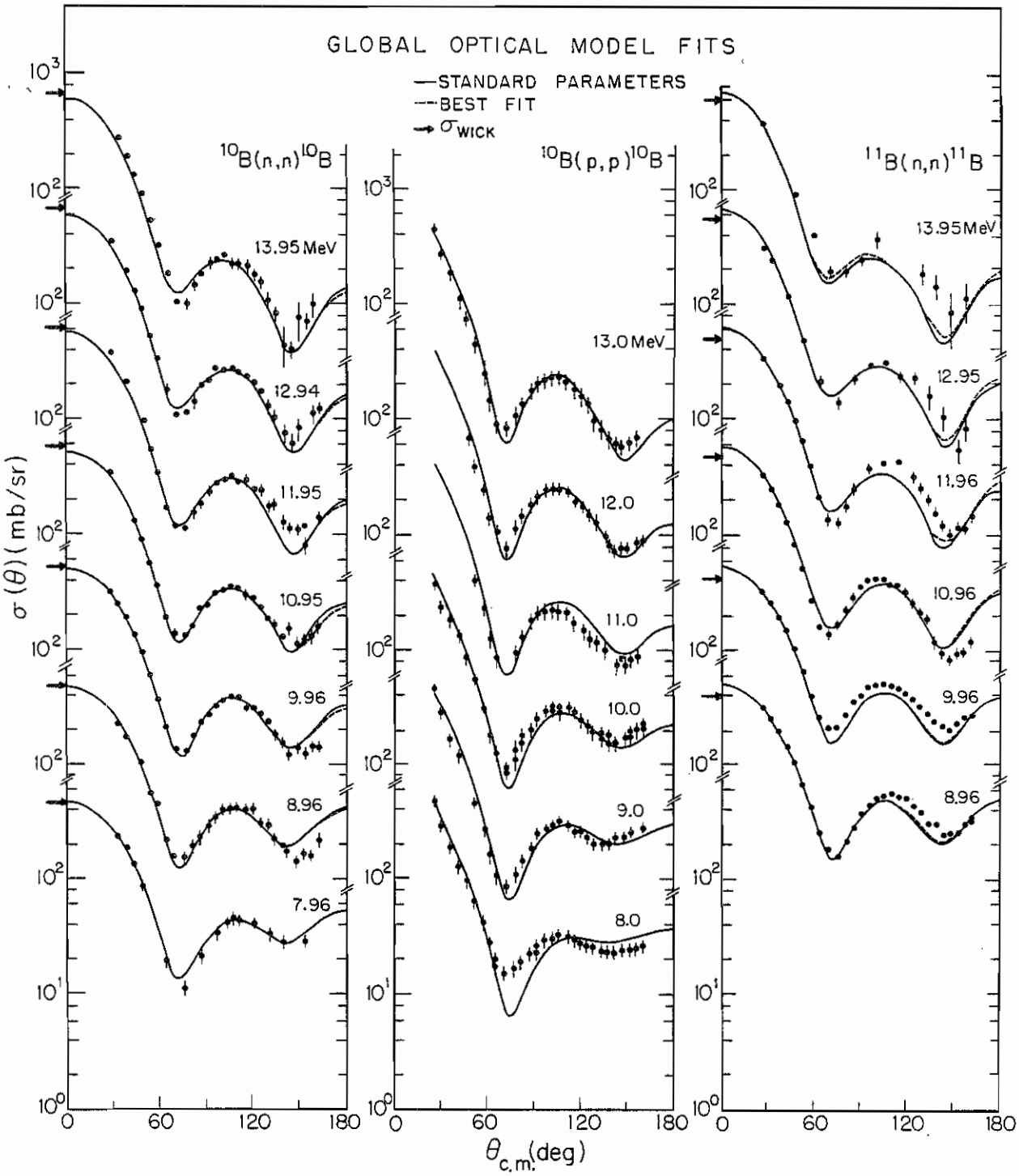
GLOBAL OPTICAL MODEL FITS
—STANDARD PARAMETERS
---BEST FIT
→ σ WICK
10B(n,n)10B
10B(p,p)10B
11B(n,n)11B
13.95 MeV
12.94
11.95
10.95
9.96
8.96
7.96
13.0 MeV
12.0
11.0
10.0
9.0
8.0
13.95 MeV
12.95
11.96
10.96
9.96
8.96
σ(θ) (mb/sr)
θc.m. (deg)
0
60
120
180

4.1.4 ^{16}O Data

The ^{16}O angular distributions were taken at energies which were near many resonances (see Figure 17). For this reason, it was not expected that a spherical optical model analysis alone would provide a very good fit to the data. The program GENOA was used to find fits to the data at En = 9.21, 10.71, 13 and 14MeV, as these energies appeared to be near minima in the total cross section. The next step was to include the resonances found in this region in the fits.

4.1.5 Resonance Parameters for ^{16}O Data

The program ANSPEC [30] is designed to add resonances to an optical model background. It is necessary in doing this that unitarity not be violated, but the program is designed to give warning if this is the case. The large resonances in the region of interest are at 10.13 MeV, 11.14 MeV and 11.54 MeV (lab energy), which correspond to excitation energies in ^{17}O of 13.67 MeV, 14.62 MeV and 14.99 MeV, respectively. Widths are estimated to be 400 keV, 340 keV and 180 keV; no spins or parities have been definitely assigned. Since the ground state of ^{16}O is a 0+ state, there are six possible J^{π} assignments for each level if J^{π}'s up to 7/2- are allowed; this means that there are 216 possible combinations of spins and parities. It is necessary to eliminate some of these to make the search practicable. Tentative spin and parity assignments have been made to the resonances

at 10.13 MeV (5/2+) and 11.54 (5/2+). Recent work by Johnson et al. [31] has been done on photoneutron reactions in ^{17}O. The levels at 13.68 MeV and 14.62 MeV in ^{17}O (corresponding to the 10.13 MeV and 11.15 MeV resonances) were found to be strongly excited in their work, which would tend to suggest an E1 transition from the ground state of ^{17}O. This would lead to J^{π} assignments of 7/2-, 5/2- or 3/2-, with 7/2- being the most strongly excited. The 11.54 MeV resonance (the 14.99 MeV level in ^{17}O) was not observed in their work, so it is likely not to be one of these strongly excited states. Thus, the first fits were tried with values for the resonances as given in Table 7.

TABLE 7

Initial Values for Resonance Parameters for ^{16}O Data

En (lab) MeV	Γ (com) keV	Γ_n keV	Ex MeV	J^{π}
10.13	400	80	13.67	7/2-
11.15	340	80	14.62	7/2-
11.54	180	50	14.99	5/2+

After the program had calculated angular distributions based on these resonance parameters and the optical model parameters found above, the optical model parameters were reevalu-

ated by finding a best set for the data at 9.2, 10.7, 13 and 14 MeV. Although the program ANSPEC has no capability for finding the best energy dependence for the parameters, it was necessary to determine the energy dependence in order to predict the optical model parameters at energies in between these minima. Accordingly, the following procedure was adopted:

1. Each of the four angular distributions was fit with the best possible set of parameters.

2. The individual geometric parameters were averaged to give a global set of geometric parameters.

3. The four angular distributions were refit using these average global parameters to find the best set of well depths (with no required systematic energy dependence).

4. These values for the well depths were fit with a straight line. This straight line was found using a simple least-squares fit program which weighted all of the points equally, and may not be the best possible energy dependence.

5. Finally, the linear fits were used to generate well depths at the intermediate energies.

The parameters so found are compared with the parameters for other p-shell elements in Table 8. The fits generated using these parameters and the resonance parameters described above are shown in Figure 23, and the predicted total cross sections in Figure 24. Also shown in this figure are the total cross sections predicted using the optical model parameters with no resonances.

For purposes of comparison, the optical model parameters found for all the elements under consideration are shown in Table 8 along with those found by Hogue. The oxygen parameters are the background parameters described above.

TABLE 8

Spherical Optical Model Parameters for some p-shell Elements

Parameter	^{6}Li	^{9}Be	^{10}B	^{11}B	^{16}O
Vo (MeV)	39.4 + 0.7Elab	42.4 - 0.5Elab	48.1 - 0.1Ecm	45.7 - 0.005 Ecm	65.8 - 1.5 Ecm
ro (fm)	1.25	1.47	1.34	1.40	1.27
ao (fm)	1.10 - 0.03Elab	0.39	0.55	0.35	0.51
Wd (MeV)	0.0 + 0.6Elab	1.0 + 0.4Elab	0.2 + 0.8 Ecm	-6.3 + 1.1Ecm	-0.64 + 0.80Ecm
ri (fm)	1.50	1.21	1.41	1.10	1.45
ai	0.88 - 0.03Elab	0.42	0.34	0.50	0.24
Vso (MeV)	5.1	4.9	5.5	5.5	5.5
rso (fm)	1.45	1.24	1.15	1.15	1.15
aso (fm)	0.59	0.35	0.57	0.57	0.57

Figure 23: Spherical Optical Model calculations for ^{16}O data using the program ANSPEC. The resonance parameters used are given in Table 7 and the background optical potential parameters are given in Table 8.

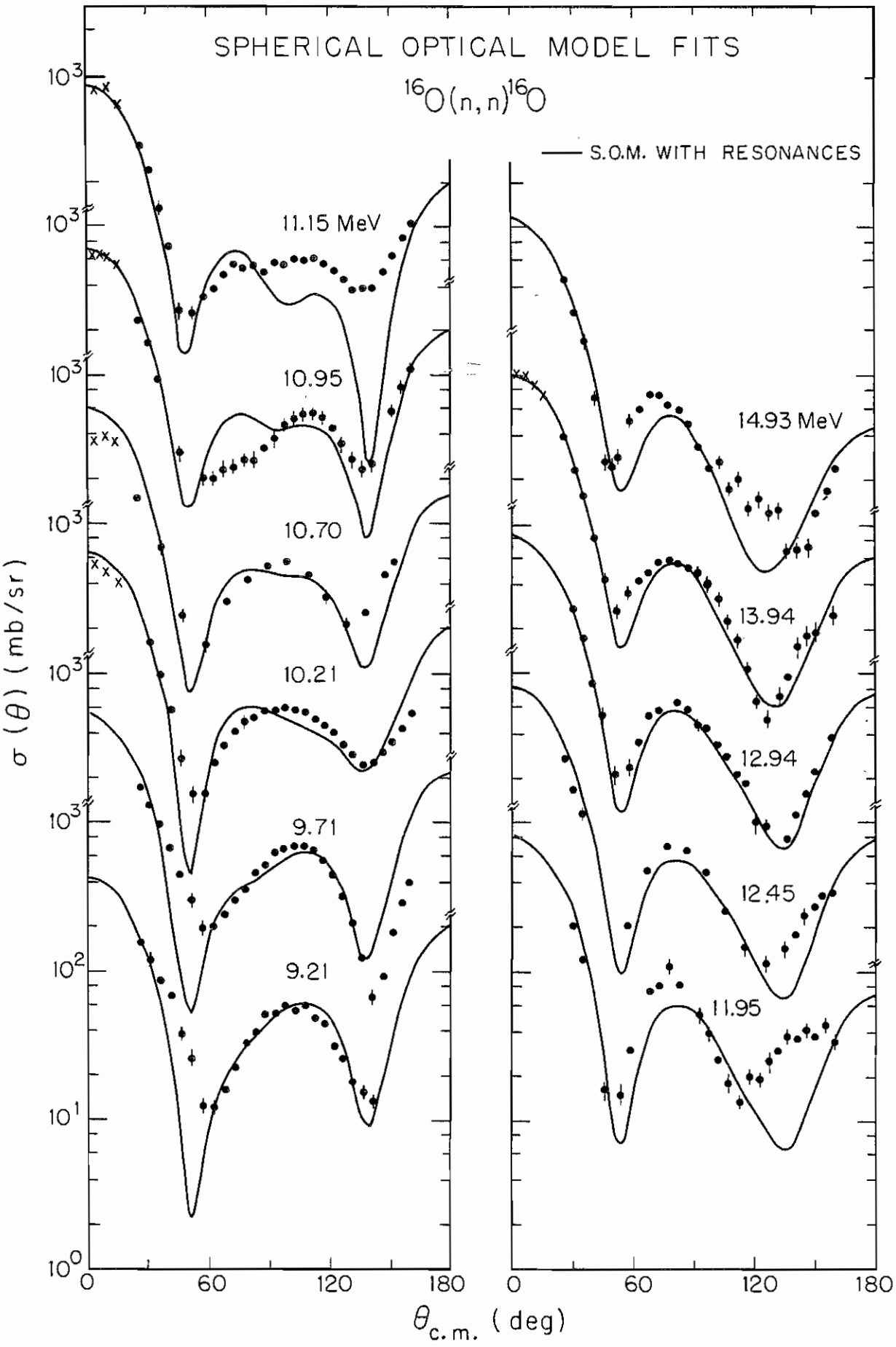
SPHERICAL OPTICAL MODEL FITS
$^{16}O(n,n)^{16}O$
S.O.M. WITH RESONANCES
11.15 MeV
10.95
10.70
10.21
9.71
9.21
14.93 MeV
13.94
12.94
12.45
11.95
$\sigma(\theta)$ (mb/sr)
$\theta_{c.m.}$ (deg)
10^3
10^2
10^1
10^0
0
60
120
180

Figure 24: Total cross section predictions for ^{16}O. The calculated values are shown along with the values from ENDF/B - IV.

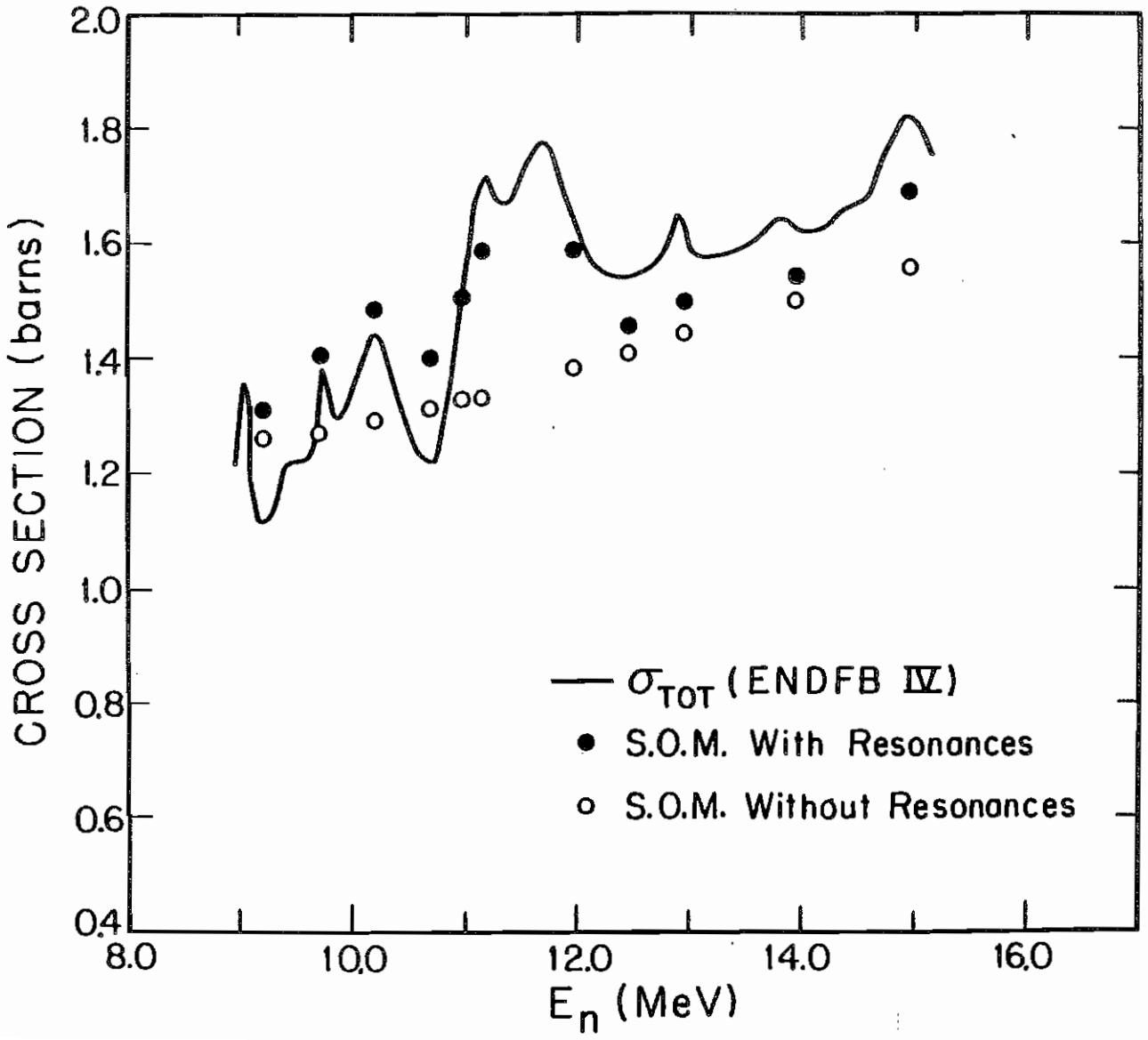
2.0
1.8
1.6
1.4
1.2
1.0
0.8
0.6
0.4
CROSS SECTION (barns)
8.0
10.0
12.0
14.0
16.0
E_n (MeV)
σ_{TOT} (ENDFB IV)
S.O.M. With Resonances
S.O.M. Without Resonances

4.2 COUPLED CHANNEL OPTICAL MODEL CALCULATIONS

It is possible to consider not only elastic scattering of nucleons but also the inelastic scattering to low-lying states. The distorted-wave Born approximation is often used to describe these data, but this treatment becomes cumbersome when it is necessary to include more than a first or second order approximation. One possible treatment used for nuclei for which the Born approximation is poor is known as the coupled-channel analysis and is discussed fully by Tamura. This analysis is particularly suited to nuclei in which some degree of collectivity is exhibited, in which the target states are described by collective coordinates. The program JUPITOR is a computer code which calculates cross sections and polarizations using a coupled-channel treatment. This powerful program has the following options of interest (among others):

1. The target nucleus can be anything, although the calculations are more meaningful for collective nuclei. Either spherical or deformed nuclei can be considered; in the former case the coupling potential is assumed to be vibrational, and in the latter it is assumed to be rotational.

2. The coupling may be either adiabatic or non-adiabatic.

3. The form factor may be either real or complex.

In the coupled-channel analysis, the optical potential is taken to be of the usual form described above, but the radii associated with the potential wells are no longer taken to be simple constants. In the spherical model, we had

$$Ro = ro * A^{1/3}$$

$$\overline{Ro} = ri * A^{1/3}$$

We will replace these with

$$R = Ro(1 + \sum_{\lambda\mu} \alpha_{\lambda\mu} Y_{\lambda\mu} (\theta,\phi)),$$

$$\overline{R} = \overline{Ro} (1 + \sum_{\lambda\mu} \alpha_{\lambda\mu} Y_{\lambda\mu} (\theta,\phi))$$

for a vibrational nucleus (which is spherical but assumed to vibrate around that shape). If the target is a rotational (permanently deformed) nucleus, R and $\overline{R}$ are

$$R = Ro(1 + \sum_{\lambda} \beta_{\lambda} Y_{\lambda 0} (\theta'))$$

$$\overline{R} = \overline{Ro} (1 + \sum_{\lambda} \beta_{\lambda} Y_{\lambda 0} (\theta'))$$

These expressions are substituted in the optical potential expressions, and the exponentials are expanded in powers of $\sum_{\lambda\mu} \alpha_{\lambda\mu} Y_{\lambda\mu}$ or $\sum_{\lambda} \beta_{\lambda} Y_{\lambda 0}$. The coupled equations obtained by defining a Hamiltonian suitable for such a non-spherical potential are solved in the program JUPITOR.

^{11}B is suitable for such analysis; it is a permanently deformed nucleus with a quadrupole moment Q = 0.0368 b. [33] The ground state and the second excited state (Ex = 4.46 MeV) are the first two members of a rotational spectrum (J = 3/2- for the ground state, 5/2- for the second excited

state). The program JUPITOR was employed to study scattering to these two states. The starting optical potential parameters were derived from the spherical optical potential parameters following the procedure advocated by Votava [32], and the value for β_2 was calculated from Q according to the tables of Löbner et al. [34]. Considerable searching on the parameters found the set given in Table 9 and plots for the two states are shown in Figure 25. For comparison, the parameter values obtained using the same method for ^{9}Be (Hogue) are also shown in Table 9.

The following should be noted about these calculations:

1. The coupling for the ^{11}B data is very weak (compared to the coupling coefficient for the ^{9}Be data). However, this weak coupling has produced a noticable decrease in the quality of the fits to the elastic data, although the fits are of the right magnitude to both inelastic and elastic data.

2. The energy dependence of the real well depth has changed drastically, although the real well radius showed no tendency to change from the value found for the spherical optical model fits.

3. The quality of the fits improves with increasing energy, although a slight decrease in the quality is seen from 11.96 to 12.96 MeV.

It is possible that the value used for the coupling coefficient, which was obtained from calculations using the hyperfine interaction, is not suitable for this application. It has been seen (Hogue, Votava) that the deformation parameter required for coupled - channel fits is a function of the incident projectile, and it may be that calculating the deformation parameter from the electric quadrupole moment gives only an average value. Further work treating this parameter as a variable may give considerable improvement in the fits.

TABLE 9

Coupled - channel Optical Model Parameters for ^{11}B and ^{9}Be

Parameter	^{11}B Value	^{9}Be Value
Vo (MeV)	71.9 - 2.9 Ecm	53.9 - 0.8Elab
ro (fm)	1.40	1.17
ao (fm)	0.35	0.54
Wd (MeV)	-3.74 + 0.58 Ecm	-0.20 + 0.54Elab
ri (fm)	1.22	1.21
ai (fm)	0.35	0.20
Vso (MeV)	5.5	4.9
rso (fm)	1.10	1.20
aso (fm)	0.57	0.31
β $(fm)^2$	-0.10	1.06

Figure 25: Coupled - channel optical model fits to ^{11}B data.

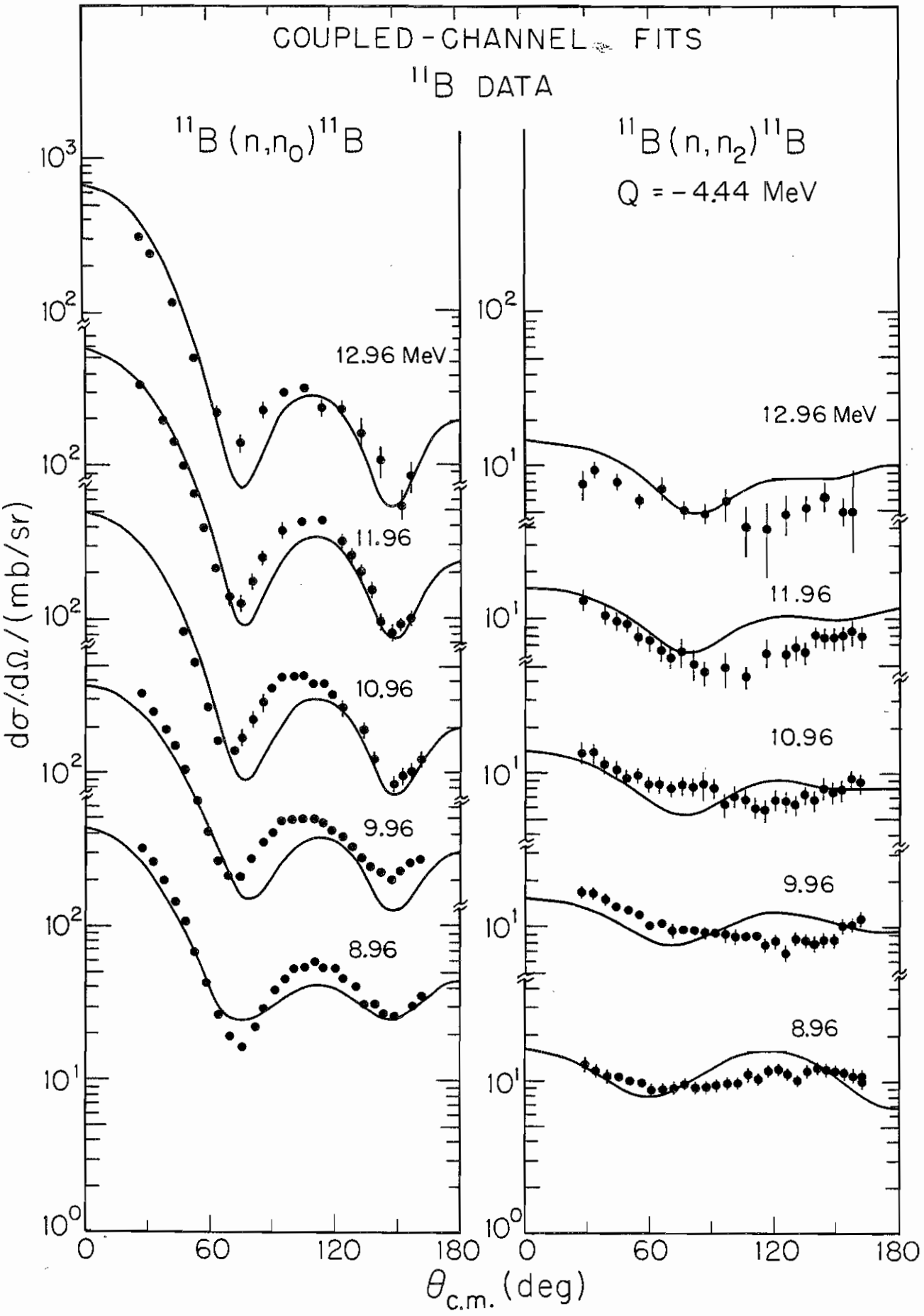
COUPLED-CHANNEL FITS
^{11}B DATA
^{11}B (n,n$_0$)^{11}B
^{11}B (n,n$_2$)^{11}B
Q = -4.44 MeV
12.96 MeV
11.96
10.96
9.96
8.96
dσ/dΩ/(mb/sr)
θ$_{c.m.}$ (deg)
0
60
120
180

Chapter V

SUMMARY

Neutron data measured in the past few years at TUNL using the NTOF facility have been studied here. The data reported consist of double - differential scattering cross sections for the p - shell elements ^{10}B, ^{11}B and ^{16}O for neutron energies between 8 and 14 MeV. Elastic scattering cross sections are reported for all three elements, together with inelastic data for various states for ^{10}B and ^{11}B. The data were studied using various forms of the optical model; specifically, the spherical optical model, the spherical optical model with the inclusion of single particle resonances, and the coupled - channel optical model.

The ^{10}B neutron data were considered along with the ^{10}B proton scattering data of Watson in order to determine the projectile isospin dependence of the scattering data. This was done by using the energy shift method of Rapaport, and it was found that very good fits to both sets of data could be found simultaneously with an energy shift of 4.6 ± 1.4 MeV energy reduction for protons. The ^{11}B data was included in the searches to determine the effect of changing target isospin in the form of the symmetry terms coefficients Vs and Ws, but the data proved to be insufficiently sensitive

to these terms to enable an accurate determination of the values of the coefficients to be made.

It was necessary to consider the ^{16}O data using a version of the spherical optical model which allowed for the inclusion of single-particle resonances. The fits to the data showed considerable improvement with the inclusion of three resonances; energies and widths of the resonances were estimated from the appearance of the total neutron cross section as a function of energy, and the spin-parity assignments were made on the basis of photoneutron studies. It is not possible to make definite assignments of spin and parity or partial widths on the basis of the data presented here, however.

The ^{11}B data were suitable for study with the coupled-channel model. The model gives good qualitative predictions for the data for the two states, but there are significant deviations from the detailed behavior of the angular distributions. It may be that further study allowing the deformation parameter to be treated as a variable parameter would improve these fits.

It is planned to undertake a study of all available nucleon scattering data from p - shell elements in this energy range to find a global set of spherical optical model parameters for these data.

Appendix A

LEGENDRE POLYNOMIAL COEFFICIENTS FOR NEUTRON CROSS SECTIONS

In the following pages the Legendre polynomial coefficients for the data presented in Chapter III section 4 are listed. The B coefficients are given, where

$$\frac{d\sigma}{d\Omega} = \frac{\sigma \text{ int}}{4\pi} * \sum_{k=1}^{k\max} \{1 + B_k * P_k (\cos(\theta))\}$$

APPENDIX A

Legendre Polynomial Coefficients for Neutron Data

Element	Energy (MeV)	Ex (MeV)	σ int (barn)	B1	B2	B3	B4	B5	B6	B7	B8	B9
^{10}B	7.96	0.0	0.887	1.377	1.831	1.729	0.839					
	8.96	0.0	0.798	1.503	1.801	1.810	0.955	0.136	0.206	0.075	0.069	
	9.96	0.0	0.878	1.649	1.923	1.914	1.033	0.135	0.048			
	10.95	0.0	0.881	1.742	2.036	2.049	1.240	0.290	1.450			
	11.95	0.0	0.906	1.874	2.257	2.196	1.332	0.396	0.138			
	12.94	0.0	0.888	1.940	2.303	2.241	1.485	0.492	0.251	0.103	0.050	
	13.95	0.0	0.887	2.038	2.454	2.321	1.620	0.560	0.327	0.103	0.086	
	7.96	0.717	0.048	-0.088	0.223							

Element	Energy (MeV)	Ex (MeV)	σ int (barn)	B1	B2	B3	B4	B5	B6	B7	B8	B9
^{11}B	7.98	0.0	1.246	1.449	1.785	0.596	0.774					
	8.96	0.0	0.931	1.314	1.645	1.673	0.846	-0.022	0.004			
	9.69	0.0	0.962	1.335	1.685	1.841	1.188	0.341	0.169			
	9.96	0.0	0.947	1.422	1.685	1.757	1.035	0.121	0.033			
	10.96	0.0	0.837	1.668	1.915	2.114	1.350	0.308	0.104			
	11.96	0.0	0.858	1.621	1.856	1.933	1.017	0.072	0.062			
	12.96	0.0	0.771	1.786	2.070	2.138	1.382	0.490	0.253			
	13.95	0.0	0.891	1.783	2.086	2.064	1.294	0.420	0.244			
	7.97	2.14	0.122	0.063	0.480							
	8.96	2.14	0.091	0.252	0.745	0.273						
	9.69	2.14	0.095	0.453	1.065	0.938	0.297					
	9.96	2.14	0.097	0.189	0.935	0.609	0.199					
	10.96	2.14	0.059	0.738	1.120	0.637						
	11.96	2.14	0.037	0.570	1.180	0.532	0.333					
	12.96	2.14	0.025	0.402	1.675							
	13.95	2.14	0.066	1.218	1.810	1.043	0.585					

7.97	4.46	0.207	-0.119	0.210	0.182	
8.96	4.46	0.132	-0.017	0.195	0.175	
9.69	4.46	0.151	0.129	0.375	-0.081	
9.96	4.46	0.135	0.408	0.415	0.125	0.207
10.96	4.46	0.108	0.360	0.390	0.042	0.198
11.96	4.46	0.091	0.360	0.715	0.098	
12.95	4.46	0.072	0.270	0.380		
13.95	4.46	0.118	-0.110	0.180		

8.96	5.04	0.091	-0.342	0.310	0.357	
9.69	5.04	0.081	-0.128	0.375	0.364	
9.96	5.04	0.063	0.159	0.465	-0.467	
10.96	5.04	0.067	0.519	1.140	0.518	0.243
11.96	5.04	0.049	0.603	1.145	0.329	0.288
12.95	5.04	0.033	0.819	0.950		
13.95	5.04	0.058	0.348	1.240		

Element	Energy (MeV)	Ex (MeV)	σ int (barn)	B1	B2	B3	B4	B5	B6	B7	B8	B9
^{16}O	9.21	0.0	0.647	0.774	0.982	1.482	1.500	-0.034	0.179			
	9.71	0.0	0.757	0.847	0.925	1.627	1.531	0.125	0.568	0.180	0.091	0.091
	10.21	0.0	0.839	0.950	1.328	1.748	1.922	0.843	0.615	0.120		
	10.70	0.0	0.684	0.624	1.250	1.175	2.044	0.688	0.540	0.313	0.128	
	10.95	0.0	0.769	0.870	1.943	1.772	2.260	0.741	1.310	0.324	0.192	
	11.15	0.0	1.132	0.984	1.725	1.727	2.067	1.058	0.987	0.237		
	11.95	0.0	1.018	1.387	1.602	1.737	2.298	1.997	0.676	0.059		
	12.45	0.0	0.793	1.513	1.702	2.029	2.637	1.867	0.843	0.447	0.278	0.224
	12.94	0.0	0.939	1.761	2.089	2.244	2.562	1.589	0.793	0.164		
	13.94	0.0	0.923	1.840	2.107	2.325	2.635	1.894	1.012	0.563	0.191	0.058
	14.93	0.0	1.111	1.942	2.274	2.432	2.789	2.266	1.506	0.477	0.129	

BIBLIOGRAPHY

1. H.H.Hogue, "Elastic and Inelastic Scattering of Fast Neutrons by ^{6}Li, ^{7}Li, ^{9}Be and ^{12}C", unpublished PhD dissertation, Duke University (1977).

2. D.W.Glasgow, F.O.Purser, H.H.Hogue, J.C.Clement, K.Stelzer, G.Mack, J.R.Boyce, D.H.Epperson, S.G.Buccino, P.W.Lisowski, S.G.Glendinning, E.G.Bilpuch and H.W.Newson, Nucl. Sci. and Eng. 61 (1976) 521.

3. H.H.Hogue, P.L.von Behren, D.H.Epperson, S.G.Glendinning, P.W.Lisowski, C.E.Nelson, H.W.Newson, F.O.Purser, W.Tornow, C.R.Gould and L.W.Seagondollar, Nucl. Sci. and Eng. 68 (1978) 38.

4. H.H.Hogue, P.L.von Behren, D.W.Glasgow, S.G.Glendinning, P.W.Lisowski, C.E.Nelson, F.O.Purser, W.Tornow, C.R.Gould and L.W.Seagondollar, Nucl. Sci. and Eng. 69 (1977) 22.

5. T.Tamura, Rev. of Mod. Phys. 37 (1965) 679.

6. T.Tamura, "Computer Program Jupitor - 1 for Coupled - Channel Calculations", ORNL - 4152 (1967).

7. H.Feshbach, Porter and V. Weisskopf, Phys. Rev. 96 (1954) 448.

8. B.A.Watson, P.P.Singh, R.E.Segel, Phys.Rev. 182 (1969) 977.

9. D.W.Glasgow, D.E.Velkley, J.D.Brandenberger, M.T.McEllistrem, H.J.Henneck and D.W.Breitenbecher, Nucl. Inst. and Meth. 114 (1974) 521.

10. F.Perey, private communication (1979).

11. L.W.Seagondollar, private communication (1979).

12. P.R.Bevington, Data Reduction and Error Analysis for the Physical Sciences, McGraw-Hill (1969).

13. J.C.Hopkins and G.Breit, Nucl. Data Tables A9 (1971) 137.

14. D.E.Velkley, J.D.Brandenberger, D.W.Glasgow and M.T.McEllistrem, Nucl. Instr. and Meth. 129 (1975) 231.

15. M.Drosg and D.M.Drake, LASL Internal Report LA-5732-MS (1974).

16. N.Jarmie, private communication (1975).

17. W.E.Kinney, Nucl. Instr. and Meth. 83 (1970) 15.

18. H.D.Knox, R.M.White and R.O.Lane, "Differential Elastic Cross Sections of Neutrons Scattered from ^{10}B for 4MeV $\leq$ En $\leq$ 8 MeV", COO-2490-5, Ohio University (1977).

19. C.E.Nelson, "A Study of the Structure of ^{12}B via Elastic Scattering of Neutrons from ^{11}B", unpublished PhD dissertation, Ohio University (1973).

20. R.M.White, R.O.Lane and H.D.Knox, "A Study of the Higher Excitation States of ^{12}B via the $^{11}B(n,n)^{11}B$ Reaction", Preliminary Report, Ohio University (1977).

21. W.E.Kinney and F.G.Perey, "Neutron Elastic- and Inelastic-Scattering Cross sections of Oxygen in the Energy Range 4.34 to 8.56 MeV", ORNL-4780 (1972).

22. C.Cowan, Evaluated Neutron Data Files/B version IV evaluation for ^{10}B, BNL (1971).

23. G.M.Hale, R.A.Nisley, P.G.Young, ENDF/B - IV evaluation for ^{11}B, LASL (1973).

24. P.Young, D.Foster jr., G.Hale, ENDF/B - IV evaluation for ^{16}O, LASL (1973).

25. R.J.Howerton and S.T.Perkins, ENDF/B - IV evaluation for ^{9}Be, LLL (1971).

26. W.P.Bucher, C.E.Hollandsworth and J.E.Youngblood, "Neutron Cross Sections for Small-angle Elastic Scattering from Nitrogen and Oxygen", BRL R 1795 (1975).

27. B.A.Watson, "The Elastic and Inelastic Scattering of Protons from ^{10}B between 5 and 16 MeV", Argonne Physics Division Informal Report PHY - 1968B (1968).

28. J.Rapaport, J.D.Carlson, D.Bainum, T.S.Cheema and R.W.Finlay, Nucl. Phys. A286 (1977) 232.

29. B.Zwieglinski, J.Piotrowski, A.Saganek and I.Sledzinska, Nucl. Phys. A209 (1973) 348.

30. W.J.Thompson, private communication (1979).

31. R.G.Johnson, B.L.Berman, K.G.McNeill, J.G.Woodworth and J.W.Jury, Phys. Rev. C20 (1979) 27.

32. H.J.Votava, T.B.Clegg, C.J.Ludwig and W.J. Thompson, Nucl. Phys. A204 (1973) 529.

33. Schaefer, Klemm and Harris, Phys. Rev. 176 (1968) 49.

34. K.E.G.Löbner, M.Vetter and V.Hönig, Nucl. Data Tables A7 (1970) 495.